On the formation of biogenic secondary organic aerosol in chemical transport models: an evaluation of the WRF-CHIMERE (v2020r2) model with a focus over the Finnish boreal forest

Giancarlo Ciarelli[1], Sara Tahvonen[1], Arineh Cholakian[2], Bruno Vitali[3], Tuukka Petäjä[1] and Federico Bianchi[1]

[1]Institute for Atmospheric and Earth System Research/Physics, Faculty of Science, University of Helsinki, Helsinki, 00014 Finland.
[2]LMD UMR CNRS 8539, ENS, École Polytechnique, Institut Pierre Simon Laplace (IPSL), Route de Saclay, 91128 Palaiseau, France.
[3] Department of Civil, Environmental and Mechanical Engineering, University of Trento, 38123 Trento (TN), Italy.

Correspondence to: Giancarlo Ciarelli (giancarlo.ciarelli@helsinki.fi)

Abstract. We present an evaluation of the regional chemical transport model (CTM) WRF-CHIMERE (v2020r2) for the formation of biogenic secondary organic aerosol (BSOA) with a focus over the Finnish boreal forest. Formation processes of biogenic aerosols are still affected by different sources of uncertainties, and model's predictions largely varies depending on the levels of details of the adopted chemical and emissions schemes. In this study, air quality simulations were conducted for the summer of the year 2019 using different organic aerosol (OA) schemes (as currently available in literature) to treat the formation of BSOA. First, we performed a set of simulations in the framework of the volatility basis set (VBS) scheme carrying different assumptions for the treatment of the aging processes of BSOA. Model's results were compared against high-resolution (i.e., 1-hour) organic aerosol mass and size distribution measurements performed at the Station for Measuring Ecosystem–Atmosphere Relations (SMEAR-II) site located in Hyytiälä, in addition to other gas-phases species such as ozone (O_3), nitrogen oxides (NO_x) and biogenic volatile organic compounds (BVOCs) measurements of isoprene (C_5H_{10}) and monoterpenes. We show that WRF-CHIMERE could well reproduce the diurnal variation of the measured OA concentrations for all the investigated scenarios (along with the standard meteorological parameters) as well as the increase in concentrations during specific heat wave episodes. However, the modeled OA concentrations largely varied between the schemes used to describe the aging processes of BSOA, as also confirmed by an additional evaluation using organic carbon (OC) measurements data retrieved from the EBAS European databases.

Comparisons with isoprene and monoterpenes air concentrations revealed that the model captured the observed monoterpenes concentrations, but isoprene was largely overestimated, a feature that was mainly attributed to the overstated biogenic emissions of isoprene. We investigated the potential consequences of such an overestimation by inhibiting isoprene emissions from the modeling system. Results indicated that the modeled BSOA concentrations increased in the northern regions of the domain (e.g., Finland) compared to southern European countries, possibly due to a shift in the reactions of monoterpenes compounds against available radicals, as further suggested by the reduction in α-pinene modeled air concentrations. Finally,

we briefly analyze the differences in the modeled Cloud Liquid Water Content (clwc) among the simulations carrying different chemical schemes for the treatment of the aging processes of BSOA. Model's results indicated an increase in clwc values at the SMEAR-II site, for simulation with higher biogenic organic aerosol loads, likely as a result of the increased numbered of biogenic aerosol particles capable of activating cloud droplets.

1 Introduction

Aerosol particles arising from the terrestrial ecosystem, referred to as biogenic aerosols, often constitute a major fraction of the observed total particulate mass (PM) (Ciarelli et al., 2016; Jiang et al., 2019b). Their contribution to PM can largely vary depending on the specific land use as well as synoptic and local meteorological conditions throughout the year (Guenther et al., 2006, 2012; Oderbolz et al., 2013).

A sub-set of particles of biogenic origin that are directly emitted into the atmosphere, e.g., pollens, mineral dust, and sea salt, are usually referred to as primary particles. They show a rather coarse particle diameters and are efficiently removed from the atmosphere via scavenging processes (Jacobson, 2005). The second group of biogenic aerosols, referred to as secondary particles, are produced in the atmosphere as a result of a series of complex chemical reactions on a time scale ranging from seconds to days (Seinfeld and Pandis, 2012).

The main precursors for the secondary organic aerosol mass originates from earth's vegetation that emits several Volatile Organic Compounds (VOCs, Guenther et al., 2012) that are usually in the gas-phase form at the most relevant ambient conditions and emissions highly depend on the local meteorological parameters (e.g. temperature, radiation, soil moisture (Guenther et al., 2012; Peñuelas et al., 2014) as well as on the specific plant ecotype. Modeling studies have shown that isoprene (C_5H_8) and monoterpenes are the most abundant organic compounds emitted from earth's vegetation (Sindelarova et al., 2014), but estimates highly depend on the model's driving variables and, in particular, on the plant functional types (PFTs) data and emissions factors (EFs) associated with them (Bergström et al., 2014). Once released into the atmosphere, VOCs can quickly (seconds to hours) react towards the hydroxyl radical ($^{\cdot}OH$), ozone (O_3) and the nitrate radical ($^{\cdot}NO_3$) to produce organic gases with a sufficient low volatility to transition into the particle phase (Xu et al., 2022). The resulting additional particulate mass is widely referred as to secondary organic aerosol (SOA), and, if produced from biogenic volatile organic compounds (BVOCs) such as isoprene and monoterpenes, to biogenic secondary organic aerosol (BSOA).

Numerous regional modeling studies, have focused on the formation and characterization of the BSOA component (Aksoyoglu et al., 2011; Bergström et al., 2012; Boy et al., 2022; Cholakian et al., 2022, 2018; Ciarelli et al., 2016; Hodzic et al., 2009; Zhang et al., 2013). However, such a highly complex system governing the formation of BSOA remains not fully understood. Initial attempts to implement the formation of secondary organic aerosol in three dimensional chemical transport models (CTMs) made used of chamber SOA yields fitted with two condensable gases to mimic the oxidation products of parent precursors, so called Odum scheme (Odum et al., 1996), as well as partition coefficients for each for the condensable gases. The Clausius-Clapeyron equation is used to adjust the saturation vapor pressure (C^*) based on temperature and using a

prescribed set of vaporization enthalpies (ΔH_{vap}). This approach has the advantage of being computationally efficient and suitable to simulate the total organic mass in a wide range of large scale (regional to global) application, but it is limited by the number of the adopted surrogate species (i.e., two) and their prescribed mean molecular weight specifications. To improve the level of details of the organic fraction in chemical transport models, the so-called Volatility Basis Set (VBS) was developed. In the VBS model, the oxidation products of a parent hydrocarbon are distributed across a wide range of volatilities, each of them with a molecular structures derived from the group-contribution approach (Donahue et al., 2011; Donahue et al., 2012). In this framework, the organic mass is binned in volatility classes, ranging from Extremely Low Volatility Organic Compounds (referred to as ELVOCs), with $C^* < 3 \times 10^{-5}$ μg m^{-3} to VOCs with $C^* > 3 \times 10^{6}$ μg m^{-3} (Bianchi et al., 2019). Such an approach allows tracking the volatility distribution of ambient organic aerosols as well as the degree of oxygenation of the organic mass (i.e., oxygen to carbon ratio). Additionally, the VBS scheme allows for further chemical reactions of primary, and secondary produced, semi-volatile organic carbon (SVOC) gases (i.e., the so-called chemical aging) available in the $0.3 < C^* < 300$ μg m^{-3} saturation concentration range. Such computational approach has been successfully applied to corroborate multiple chamber aerosol chemical aging studies that revealed an further increase in SOA concentrations when first-generation oxidation products were further reacted against the $^{\cdot}OH$ radical (Donahue et al., 2012).

On a global scale, Tsigaridis et al., 2014 compared model simulations of thirty-one chemical transport models and general circulation models (GCMs) in the framework of the AeroCom phase II. Their results indicated that model simulations of OA greatly vary between models, mainly due to the increasing complexity of the SOA parameterization and the addition of new OA sources in recent years. In Europe, a growing number of chemical transport modeling studies have been performed with a focus on the BSOA fraction of OA. Bergström et al., 2012 tested the aging of BSOA in the EMEP model using aging reaction rates constant as proposed by Lane et al., 2008 (i.e. 4.0×10^{-12} cm^3 $molecule^{-1}$ s^{-1}). Model's results were evaluated against measurements data available during 2002 and 2007 mainly using filter measurements of organic carbon (OC) as available at different EMEP rural background sites (at daily and weekly time resolution). Their results suggested that, compared to other aging schemes, accounting for aging reactions of BSOA (PAA method in Bergström et al., 2012) improved model prediction of OC during summertime and at the majority of the sites. Similarly, Zhang et al., 2013 deployed the CHIMERE model with two nested domains covering Europe and Northern France. Aging of BSOA were identical to the aging of the anthropogenic secondary organic aerosol (ASOA) i.e. 1.0×10^{-11} cm^3 $molecule^{-1}$ s^{-1} (Murphy and Pandis, 2009), and biogenic emissions were driven with the Model of Emissions of Gases and Aerosols from Nature (MEGAN) model (Guenther et al., 2006). Model simulations of OA were performed for the MEGAPOLI summer campaign of July 2009 and compared against 1-hour aerosol mass spectrometer (AMS) data available in the Greater Paris area (1 urban and 2 suburban sites). Their results indicated that accounting for aging of both anthropogenic and biogenic SVOCs helped to improve the agreement between modeled and observed OA, particularly in terms of the temporal variabilities and occurring times of major pollutions peaks. Long-range related air masses, however, were overestimated in the model, possibly because of the too aggressive aging chemical scheme in the model. These results were additionally confirmed by a later application of the CHIMERE model during the ChArMEx 2013 campaign conducted in the western Mediterranean basin, i.e. Ersa, Cap Corse (Corsica, France) (Cholakian et al., 2017).

Comparison of modeled and observed OA concentrations indicated a large overestimated of the OA fraction in the model when aging of BSOA were implemented following the same pathway as ASOA (i.e., K_{OH} = 1.0 × 10^{-11} cm^3 $molecule^{-1}$ s^{-1}), suggesting a too aggressive production of low-volatile gases available to rapidly transition in the particle phase. Therefore the author also tested a fragmentation schemes in their VBS model where the oxidation products of the parent hydrocarbon were allowed to fall in an higher saturation vapor pressure range (compared to the parent precursor, i.e. fragmentation), and using a branching ratio for the distribution of the products, i.e. 75% fragmentation and 25% functionalization (Shrivastava et al., 2015). Model results indicated a large reduction in the model positive bias compared to simulation with non-fragmentation processes and aging of BSOA.

In this study, we focus on the formation and aging processes of BSOA as an important fraction of the total OA in areas that are affected directly, and largely, by biogenic emissions, i.e., the Finnish boreal forest. As new high temporal resolution measurements of OA and biogenic gas-phase compounds are now available, we evaluate 1) the effect of BSOA chemical aging in the WRF-CHIMERE model, 2) the model performance with respect to BVOC emissions, meteorological parameter, photochemistry (i.e. NO_x and O_3) and OA mass at the Station for Measuring Ecosystem–Atmosphere Relations (SMEAR-II (Hari and Kulmala, 2005) site, 3), the sensitivity of OA formation in the model with respect to isoprene emissions, and in particular on BSOA, and 4), the changes in the modeled Cloud Liquid Water Content (clwc) when the treatment of the aging processes of BSOA is accounted for. To provide a more comprehensive analysis of the simulations, model's results are additionally evaluated against observational data from two European databases, i.e., EBAS and the Air Quality e-Reporting (AQ e-Reporting) database.

2 Method

2.1 The WRF-CHIMEREv2020r2 Model

The WRF-CHIMEREv2020r2 model, WRF-CHIMERE thereafter (Menut et al., 2021), is a three dimensional CTM capable to simulate physical and chemical processes taking place into the atmosphere, from the injection of emissions in the planetary boundary layer (PBL), to chemical reactions of hundreds of chemical compounds to dry and wet deposition processes. The CHIMERE model has participated in numerous intercomparison exercises (Bessagnet et al., 2016; Ciarelli et al., 2019; Solazzo et al., 2017; Theobald et al., 2019) and it is an active member of the Copernicus Atmosphere Monitoring Service (CAMS) operational ensemble. Recently, it has been upgraded to run "online" with the Weather Research and Forecast (WRFv3.71) model to include the exchange of the aerosol size distribution, among other parameters, between CHIMERE and the meteorological model, i.e. WRF (Briant et al., 2017; Tuccella et al., 2019). It can be applied at various horizontal resolutions, and it is therefore suitable for both global (hundreds of kilometers) and urban (1 km) scale applications (Bessagnet et al., 2017; Mailler et al., 2017).

Simulations were performed for the summer of 2019 (i.e., from 15 June 2019 until 31 August 2019) using two domains on a Lambert conformal projection: a first domain covering whole Europe at about 30 x 30 km resolution and a second nested domain centered over Finland at about 10 x 10 km resolution (Figure 1). The chemical mechanism used for the gas-phase chemistry was the MELCHIOR2 scheme (Derognat, 2003), including up to about 120 reactions with updated reaction rates (last updated in 2015). The ISORROPIA thermodynamic model was used to calculate the partitioning of the inorganic aerosol constituents (Nenes et al., 1998) and a logarithmic sectional distribution approach was deployed to treat the size distribution of aerosol particles using 15 bins ranging from 10 nm to 40 µm. The model additionally account for coagulation process (Debry et al., 2007) as well as binary nucleation of sulfuric acid (H_2SO_4) and water (Kulmala et al., 1998). The treatment of OA in the model, and specifically of BSOA in the framework of the VBS scheme, is described in detail in the next section.

2.2 OA schemes

The VBS scheme was first implemented in the CHIMERE model for the Mexico City metropolitan area during the MILAGRO field experiment (Hodzic and Jimenez, 2011); however, the version included in the model is the one developed and applied over Europe for the Metropolitan area of Paris (Zhang et al., 2013). Oxidation products of BVOCs are distributed into four classes of volatility at saturation concentrations of 1, 10, 100, and 1000 µg m^{-3} (at 300 K) with different mass yields for low-NO_x and high-NO_x conditions based on the work of Hodzic and Jimenez, 2011, and reference therein, and allocated in a dedicated set to uniquely track their contribution to OA (Figure 2). All monoterpenes species have identical SOA yields, but specific reactivities based on Bessagnet et al., 2008. The model employs a simplified treatment for the formation of BSOA from sesquiterpenes. BSOA from sesquiterpenes is considered only for the reaction against the $^{\cdot}OH$ radical, and oxidation products distributed in the same volatility bins used for the rest of the BSOA precursors, and with not differentiation between

low-NO_x and high-NO_x conditions. The reaction rate of sesquiterpenes (i.e., humulene lumped class) against OH is set to 2.9 x 10^{-10} molecule^{-1} cm^3 s^{-1} with mass yields taken from Tsimpidi et al., 2010. The resulting gas-phase material, can be further oxidized in the model by the ·OH radical (blue curved arrows in Figure 2) resulting in an increase of 7.5 % in the organic mass to mimic the addition of an oxygen (Robinson et al., 2007) and in a simultaneous shift in volatility by one order of magnitude. In this VBS schemes, also referred to as 1D VBS schemes, a fixed molecular structure, and therefore molecular weights, is assigned to each of the four volatility classes, i.e., 180 g mol^{-1}. The effective enthalpy of evaporation (ΔH_{vap}) of each BSOA volatility class is unique and set to 30 kJ mol^{-1}. Additional formation of BSOA from O_3 and NO_3 is taking into account following the same approach as in Murphy and Pandis, 2009 (Menut et al., 2021; Zhang et al., 2015, 2013).

Aging of biogenic aerosol have been tested in previous modeling application at European scale (Bergström et al., 2012; Cholakian et al., 2017; Zhang et al., 2013). However, very few of these studies have investigated the effects and impacts of using difference biogenic aging scheme in an environment that is largely affected by biogenic emissions and by combining parallel state-of-the-art measurements of a vast array of atmospheric compounds. In this study we performed a comprehensive evaluation of the difference aging schemes as currently available from the literature. Specifically, we tested the oxidation of gas-phase biogenic organic material in the SVOC range, i.e., chemical aging, (blue curved arrows in Figure 2). Additionally, we also tested the influence of isoprene emissions on BSOA formation (Table 1). In total, we performed four simulations, as described below:

- Aging-On-Case-1: Gas-phase organic material of biogenic origin in the SVOC range can react with the ·OH radical with a reaction rate of 1 x 10^{-11} molecule^{-1} cm^3 s^{-1} (Murphy and Pandis, 2009; Zhang et al., 2013).
- Aging-On-Case-2: Gas-phase organic material of biogenic origin in the SVOC range can react with the ·OH radical with a reaction rate of 4 x 10^{-12} molecule^{-1} cm^3 s^{-1} (Bergström et al., 2012; Lane et al., 2008). This simulation also represents the base-case simulation for the evaluation of both meteorological parameters and the photochemistry.
- Aging-Off: Gas-phase organic material of biogenic origin in the SVOC range does not further react with the ·OH radical. SVOC species are included in the partitioning equations and/or removed from the system via wet and/or dry deposition.
- C_5H_8-emissions-Off: Emissions of C_5H_8 are inhibited in the emissions model (i.e., MEGAN). Gas-phase organic material of biogenic origin in the SVOC range can react with the ·OH radical with a reaction rate of 4 x 10^{-12} molecule^{-1} cm^3 s^{-1} (Bergström et al., 2012; Lane et al., 2008), i.e. based on Aging-On-Case-2.

Formation of ASOA is included by using the same range of volatilities as for BSOA. Aging of ASOA is accounted for in our application with a reaction rate of 1 x 10^{-11} molecule^{-1} cm^3 s^{-1} (Murphy and Pandis, 2009; Zhang et al., 2013). This value is not altered across all the sensitivity tests. SVOCs arising from the evaporation of POA upon dilution are allowed to age with a reaction constant of 4 x 10^{-11} molecule^{-1} cm^3 s^{-1} (Robinson et al., 2007) and no acid enhanced BSOA production and anthropogenic pollution-enhanced SOA production is accounted for. No volatility dependence of the Henry's law water solubility coefficients is included.

2.3 Input data

Annual anthropogenic emissions of black carbon (BC), organic carbon (OC), carbon monoxide (CO), ammonia (NH_3), non-methane volatile organic compounds (NMVOCs), nitrogen oxides (NO_x) and sulfur dioxide (SO_2) were retrieved from CAMS for the whole year 2019 at 0.1 x 0.1 degree resolution and hourly distributed over the investigated periods (summer of 2019) with temporal profiles based on the EMEP MSC-W model (Simpson et al., 2012). Biogenic emissions of NO, isoprene, limonene, α-pinene, β-pinene, ocimene, and humulene (representing the lumped class of sesquiterpenes) were prepared using the MEGAN model version 2.1 (Guenther et al., 2012). Emission rates of 15 plant functional types (PFTs), at an original horizontal resolution of 0.008º × 0.008º, were re-gridded to match the resolution of both the coarse and high-resolution nested domains (i.e., 30 km and 10 km, respectively). Standard emissions rate are adjusted based on several environmental factors, based on local radiation and temperature values (among others variables such as leaf area index (LAI), Guenther et al., 2006). No emissions from wildfires were included in the simulations. Meteorological input were simulated with the WRF regional model (v3.71) (Skamarock et al., 2008) forced by National Centers for Environmental Prediction (NCEP) Climate Forecast System Version 2 (http://www.ncep.noaa.gov, last access: 20 February 2023) with a temporal resolution of 6 h, an horizontal resolution of 1 degree, and with the course domain nudged towards the reanalysis data (every 6 hours, i.e. surface grid nudging). Simulation were performed using the Rapid Radiative Transfer Model (RRTMG) radiation scheme (Mlawer et al., 1997), the Thompson aerosol-aware MP scheme to treat the microphysics (Hong et al., 2004) the Monin–Obukhov surface layer scheme (Janjic, 2003), and the NOAA Land Surface Model scheme for land surface physics (Chen and Dudhia, 2001).

Initial and boundary conditions of aerosols and gas-phase constituents were retrieved from the climatological simulations of LMDz-INCA3 (Hauglustaine et al., 2014), where a monthly average of several years is created on a global level and used as boundary conditions for the coarse domain, and the Goddard Chemistry Aerosol Radiation and Transport (GOCART) model (Chin et al., 2002). For aerosol species the model includes inorganic species such as fine and coarse nitrate, ammonium, sulfate, dust, as well as OC and BC.

3 Observational data and model evaluation methods

Observational data were taken from at the SMEAR-II station located within the boreal forest of Finland (black cross in Figure 1). Common meteorological parameters with a temporal resolution of 1-hour were used to evaluate the performance of the WRF model, i.e., surface temperature, wind speed, wind direction, relative humidity, and precipitation.

The CHIMERE model was evaluated with gas-phase measurements of isoprene, monoterpenes, ozone, and nitrogen oxides (in dry air) taken at 4.2 meters on a 1-hour temporal resolution. Nitrogen oxides measurements were performed with a chemiluminescence analyzer (TEI 42 CTL) whereas ozone measurements were performed with the ultraviolet light absorption analyzer (TEI 49 C). Measurements of isoprene and monoterpenes BVOCs were performed with the proton transfer reaction-mass spectrometry (PTR-MS, Rantala et al., 2015).

The modeled total organic aerosol mass (OA) was compared against Aerosol Chemical Speciation Monitor (ACSM) measurements available during the summer of 2019 (i.e., from 15 June 2019 until 31 August 2019). The ACSM measures the non-refractory (NR) sub-micrometer particulate matter mass (i.e., material evaporating at 600º) with an aerodynamic diameter less than 1 µm (PM_1). A complete description of the ACSM measurements is available in Heikkinen et al., 2021. Finally, the modeled particle size distribution was compared against Differential Mobility Particle Sizer (DMPS) measurements.

Additional measurements of OC and isoprene air concentrations were taken from the EBAS European database (https://ebas.nilu.no/) (Table S1 and Table S2). NO_x and O_3 measurements were retrieved for rural stations as available from the Air Quality e-Reporting (AQ e-Reporting) database (https://www.eea.europa.eu/en). Specifically, 271 stations were retrieved for NO_x and 350 stations for O_3. Observations at these sites were compared against model data from the coarse grid (at 30 km). The statistical metrics used for the meteorological and chemical performance evaluation is reported in Table 2.

4 Results

4.0 Synoptic context

The summer of 2019 was the second warmest on global scale and was among the 5 warmest measured in Europe since the 16th century, producing a regional temperature anomaly close to 2 K (compared to 1981-2010), comparable to that of 2003 (Sousa et al., 2019). Two distinct severe heat wave events occurred during the period considered in this study, the first in late June and the second in late July. Both events were characterized by the presence of a low-pressure system in the North-eastern Atlantic and a ridge extending over Europe, causing persistent anticyclonic conditions, low cloud cover and warm sub-tropical air advection from northern Africa, a configuration typically associated to extreme temperatures (Tomczyk et al., 2017). The synoptic pattern of the late June heat wave was better defined, and affected mainly southwestern Europe, while the late July heat wave could reach further northward toward Scandinavia, affecting also Finland, where a record temperature of 33.2º was measured on the 28th (Villiers, 2020). Besides the dynamical influence, the first event was enhanced by vertical descent of potentially warmer air. Differently, the late July heat wave was driven by diabatic fluxes and surface-atmosphere coupling, a process amplified by the soil moisture deficit produced by the first extreme event (Sousa et al., 2019). In Figure 3 we show the large-scale configuration of the late July event, which strongly affected Finland. On the 19th the high pressure was already located on the Iberian Peninsula and started to expand northwards. On the 25th the strongest pressure and temperature anomalies were registered in France and Spain, and the ridge started to influence northern Europe. After the 26th the Atlantic low moved East across Great Britain bringing cooler air to continental Europe, which was however still affecting Scandinavia. On the 29th Finland started to be influenced by western cold continental air.

4.1 Analysis and evaluation of meteorological parameters

Meteorological conditions are a fundamental ingredient to understand the formation, transportation and removal of pollutants (Bianchi et al., 2021; Seinfeld and Pandis, 2012). However, there are not always simultaneously analyzed in CTM applications, and often uncertainties are presented relatively to the underlying gridded emissions and/or chemical mechanics. It is therefore important to also characterize the meteorological conditions and evaluate the key meteorological parameters that are driving the physical and chemical processes.

Figure 4 and Table 3 reports the comparison between modeled and observed meteorological parameters at the SMEAR-II station. The site was characterized by rather warm temperatures during the very beginning of the simulations, which later transitioned into a colder period persisting until about 15 July. Afterwards, a sustained increased in temperatures occurred between around the 18 and 29 of July (with daytime temperatures well above 20º) after which the temperatures dropped again until the end of the period. The model was able to reproduce such a temporal trend with a slight underestimation (-0.7º) occurring mainly during the nighttime periods (Figure 4). A comparison between modeled and observed relative humidity also

indicated similar level of agreement with the diurnal variation well captured in the model, but some sporadic short-lived rain events were missed by the model.

The analysis of the wind direction fields indicated that they were satisfactorily reproduced by the model, with the southern westerly (SW) sector being the most predominant wind direction during the summer period (r = 0.5), but with wind speed generally over predicted. Quite low wind speed values (i.e., around 1 - 1.5 m s^{-1}) were observed during the middle of simulation (from the 18 to the 29 of July) concurrently with "heat wave" episode, whereas values were generally higher (2 - 2.5 m s^{-1}) during the first half and second half of the investigated periods, a pattern that the model well reproduced (r = 0.62).

4.2 Analysis of biogenic volatile organic compounds (BVOCs)

We report here the analysis of the biogenic emissions fluxes (i.e., output from the MEGAN model) for monoterpenes, isoprene, and sesquiterpenes (humulene lumped class) emissions as well as the comparison of their corresponding air concentrations (i.e., output from the CHIMERE model). Figure 5 shows the average spatial distribution of monoterpenes and isoprene BVOCs for the investigated period and for the 10 km resolution nested domain centered over Finland. As expected, monoterpenes emissions clearly dominate the biogenic emission flux over isoprene with a north to south gradient. The model indicated few localized areas, mainly in the eastern regions of the domain, where substantial isoprene emissions are evident. Specifically, at the location of the SMEAR-II station, isoprene emissions show a larger diurnal variability compared to monoterpenes (Figure 6) with model predicting up to about 59, 36 and 5 % of monoterpenes, isoprene and sesquiterpenes (humulene) relative contributions to the total BVOCs pool, respectively (Figure 7).

Previous model estimation of biogenic emissions over the Finnish forest indicated than monoterpene emissions dominates the total BVOC pool, representing up to about 45 % of the annual total emission whereas isoprene emissions contribute by about 7 % (Lindfors and Laurila, 2000), which is considerably lower than the isoprene relative contribution reported here. Those discrepancies can likely arise from the different EFs, and land use types, that are used to retrieve the biogenic emission fluxes. Even though the underlying emission mechanism is very similar compared to the one used in previous studies (Guenther, 1997), the emission factors applied to those early estimates of biogenic flux were specifically retrieved for boreal tree species, different from the one used here which are directly taken from measurements available in north America and Central Europe. Additionally, in those previous studies, tree species with no documented isoprene emission were assigned a minimum emission rate, whereas in this work we applied EFs as implemented in the MEGAN modeling framework (Guenther et al., 2006).

The comparisons of isoprene and monoterpenes air concentrations at the SMEAR-II station is reported in Figure 8. The model could reproduce relatively well the concentrations of monoterpenes with increasing values occurring during the warmer periods of the investigated period (denoted here as "heat wave") and relative lower values during the colder periods (see Section 4.1). Few isolated spikes in monoterpenes air concentrations are likely to arise from local anthropogenic activities in the nearby sawmill facilities (Heikkinen et al., 2021; Hellén et al., 2018; Vestenius et al., 2021), a feature that is not included in the emission model. Modeled sesquiterpene concentration were found to be around 15 ppt on average for the investigated periods,

which is comparable the total detected sesquiterpenes average concentrations reported by Hellén et al., 2018 for the summer of 2016. Isoprene concentrations also indicated an increase in concentrations during periods characterized by warmer temperatures, but concentrations were largely overestimated. The ratio between the modeled and observed isoprene air concentration varies from 4 to 8, with few isolated peaks exceeding a factor of 10 (Figure 8). An additional comparison with isoprene air concentration data as available from the EBAS database indicated that the overestimation is systematic across most of the European sites (Figure S1). Specifically, the model shows an overestimation of isoprene at 70% of the analyzed stations. It is interesting to notice that also for the additional station located in Finland, i.e., Pallas (FI0096G) the model indicated a substantial overprediction of isoprene emissions (Figure S1), therefore indicating that the problem might be more accentuated for European boreal forests. This is also confirmed by a very recent global modeling study presented by Zhao et al., 2023 where the GEOS-CHEM model was applied over the northern high latitudes (Zhao et al., 2023). Overestimations of isoprene in CTM application with the MEGAN model at the SMEAR-II were also reported in the study of (Jiang et al., 2019a), which used the Comprehensive Air Quality Model with Extensions (CAMx) model to simulate the entire year of 2011, and, more recently, in a WRF-CHIMERE application over the pine forest in south-western France (Cholakian et al., 2022). Even though the models use different chemical schemes to perform the gas phase and particle phase chemistry, they both indicated a large overestimation of isoprene concentrations, also at other European sites. The implications of such an overestimation in isoprene biogenic emissions is analyzed in detail in Section 4.5.

4.3 Analysis and source apportionment of OA

The modeled total OA fraction is compared against OA measurements performed with the ACSM instrumentation (Heikkinen et al., 2021). In the model, this fraction represents the sum of POA (i.e., primary emitted organic material) and SOA (i.e., secondary formed organic material upon oxidation and subsequently condensation of the resulting low-volatile vapors) from all the sources considered in the simulation (biogenic, anthropogenic as well as boundary conditions). Figure 9 reports the hourly and diurnal comparisons for all the three BSOA schemes under evaluation. Specifically, the model can reproduce the temporal trends of the observed OA fraction relatively well: the three main peaks occurring during the beginning, the “heat wave” and the last week of the investigated periods are all captured, but their magnitude highly depends on the specific BSOA scheme (Table 1). We additionally compared model data against organic carbon (OC) measurements as available from 15 additional EBAS sites (Table S1) and at different time resolution (from 4 hours to 1 week). Since the model uses the organic aerosol (OA) mass concentration in its own calculations, we applied the OA/OC ratio as in Bergström et al., 2012. Results indicated similar behaviors also for OC data (Figure 10) with the model showing a substantial increase in the OC mass and with larger overestimation for aging schemes that account for very aggressive aging processes. The mean bias varies from 0.63, -0.13 and -1.1 for the Aging-On-Case1, Aging-On-Case2 and Aging-off case, respectively (Table S3).

Additionally, periods with relative low concentrations are also well reproduced, with no substantial positive bias observable. The analysis of the diurnal profiles indicates that the model can reproduce the daily variation, with a rather flat diurnal variation

of OA concentrations which increase slightly during nighttime and early morning hours. Extremely low OA concentrations are missed by the model (Figure 9). The latest might suggest uncertainties in the background OA fields used in the model and/or in the concentrations injected at the very boundaries of the coarser domain (i.e., long-range transport).

The model-based source apportionment of the OA fraction for the three different BSOA schemes is reported in Figure 11 and Figure 12 for the entire domain as well as for the SMEAR II station. As expected, not much of a difference is noticed for the POA and anthropogenic secondary organic aerosol (ASOA) concentration for the different aging scheme, with POA contributing largely over the urban areas of Helsinki, Turku, and over the city Tallinn and Saint Petersburg, with average concentration up to about 0.5 μg m^{-3} on average. The model-based source apportionment predicted ASOA concentrations to exceeded POA ones, sometimes also in urban areas, like for example over the urban area of Helsinki, and in general, in the southern part of the domain where concentrations are relatively higher compared to northern regions (up to about 1.5 μg m^{-3}). BSOA concentrations, on the other side, were predicted to be more heterogeneously distributed within the domain (inner domain), and the OA mass largely increases as aging processes are increasingly accounted for. For instance, in the Aging-Off scenarios, concentrations reach a maximum of around 1 μg m^{-3} on average over the whole period, whereas in the Aging-On-Case-1 case they reach up to 3 μg m^{-3} on average. This represents a substantial difference in the modeled BSOA mass, which is mainly driven by periods characterized by higher temperatures and therefore higher photochemical activity (Figure 9).

The pie chart In Figure 12 reports the modeled average relative contribution of the OA fraction at the SMEAR-II site. Each of the three parameterizations indicated that the secondary fraction of OA is the dominant one, which is also in agreement with the positive matrix factorization (PMF) analysis performed on the ACSM data (Heikkinen et al., 2021). In the latter, a statistical source apportionment study of the OA measurement data was performed using the spectral profiles from the ACSM. The authors were able to identify three categories of OA: low-volatility oxygenated OA (LV-OOA), semi-volatile oxygenated OA (SV-OOA), and primary OA (POA). Their results indicated that LV-OOA and SV-OOA almost accounted for the entire OA mass during the summer periods (and eventually also during winter periods), with LV-OOA being the dominant component throughout the entire year. On the other side, the highest SV-OOA contribution to the OA mass was identify during summer periods (about 40%) with a distinct diurnal cycle with peaks in the early morning and in the late evening (in line with the diurnal profiles indicated by WRF-CHIMERE, Figure 9). Nevertheless, comparison of the PMF-retrieved SV-OOA and LV-OOA components against WRF-CHIMERE data is currently challenging because of the limited number of volatility bins used in the model to describe the formation of BSOA (i.e., currently limited to 4 at 1, 10, 100, and 1000 μg m^{-3} at 300 K), which only partially cover the low-volatile range (Bianchi et al., 2019). This limitation was further investigated by comparing the model size distribution with DMPS measurements at the SMEAR-II site. The model largely overestimates the number of particles below 100 nanometers and underestimate the accumulation mode (Figure S2). These behavior were already reported in the work of Tuccella et al., 2019 which used aircraft measurement data (available both in the PBL and in the free-troposphere) to evaluate the model size distribution. Whether we acknowledge that this model version does not account for any adjustment of the organic compounds based on their size, i.e. Kelvin effect (which will reduce the amount of semi-volatile compounds condensing on very small particles size, mainly below the 10 nanometers sizes), and that the number of particles

is retrieved in a prognostic manner from the total OA mass, density, and particle diameter, it is likely that the lack of a more explicit representation of the LVOC and ELVOC compounds (i.e. volatility bins) in this VBS framework (Figure 2) could potentially reduce the growth, by condensation, of particle in the lower end of the size distribution, therefore adding to the overestimation in the smaller diameters and to the under prediction of the larger ones (which will additional reduce the coagulation efficiency of smaller particles towards larger sizes).

Finally, the model-based relative contribution of ASOA and BSOA to the total OA mass indicates substantial variations depending on the adopted chemical scheme. For the Aging-Off test the model predicted up to 43 % contribution of the anthropogenic SOA fraction to the total OA mass, which is very likely overestimated for the SMEAR-II boreal site. The aging of BSOA yield results that are more reasonable both in the terms of the contribution of the single OA components and also in the terms of the absolute concentrations (for the Aging-On-Case-2 BSOA scheme), i.e. with the BSOA fraction contributing up to 72 % to the total OA and the total OA mass negatively biased by 0.7 μg m^{-3} (Table 5).

4.4 Impacts on cloud liquid water content (clwc)

We report a preliminary analysis for the changes in modeled Cloud Liquid Water Content (clwc) between the different aging schemes. As discussed in the Section 2.1, we run the model in "online" configuration, therefore allowing CHIMERE to pass the diagnosed particle size number distribution, aerosol bulk hygroscopicity, ice nuclei (IN) and deliquesced aerosol to the WRF model. CHIMERE chemical and physical parameters were passed to the WRF model with an exchange frequency of 20 minutes and the aerosol activation to cloud droplets treated with the Abdul-Razzak and Ghan scheme (Abdul-Razzak, 2002) using a similar approach available in the WRF-Chem model (Chapman et al., 2009). More details on the Aerosol-Cloud Interaction within WRF-CHIMERE can be found in (Tuccella et al., 2019).

Figure 13 reports the vertically integrated average relative changes in clwc between the Aging-On-Case-2 and Aging-Off schemes for the entire simulation period. We calculated these differences using the Aging-On-Case-2 scenarios since it yields the best results against OA measurements (Section 4.3). We reported the vertical distribution of aerosol particles up to 150 nanometers, i.e., including particles that can effectively act as cloud condensation nuclei (CCN), as in the Aging-On-Case-2 and Aging-Off cases. Generally, the model indicated an increase in the clwc when the aging of biogenic aerosols are accounted for, owing to the increase in the biogenic aerosol mass loading (Figure 10) and therefore of the number of biogenic particles that can act as CCN (Figure S2). Changes in clwc are predicted to be larger over the land, and especially in the central region of the domain and over the SMEAR-II site where the model indicates around 30% increase in clwc in the Aging-On-Case-2 respect to the Aging-Off. Most of the changes, i.e., total number of particles up to 150 nanometers and clwc, occurred below about 1000 meters above sea level (a.s.l). which is roughly the estimated average PBL height during summer period at SMEAR-II (Sinclair et al., 2022), with larger increases, in both particles number and clwc, slightly below the 1000 m a.s.l altitude. Climatic feedbacks from biogenic particles over boreal area were very recently reported in Yli-Juuti et al., 2021 by the means of remote sensing and ACSM observations available at the SMEAR-II stations. Specifically, the analysis indicated

an increase in OA loading, and CCN, during the 2012 - 2018 periods as results of the increase in surface temperature. Higher cloud optical depth data were also statistically significantly associated with higher OA loading, providing direct evidence for the indirect effect of biogenic aerosols. The model results presented here, seem to be in line with such results, but a separate study is needed to analyze in greater detail the modeled indirect effect under longer periods of time (i.e., model trend analysis).

4.5 Sensitivity of BSOA formation to C_5H_8 emissions

We discuss in this section sensitivity analysis with inhibited isoprene biogenic emissions. As presented in the previous section, modeled isoprene air concentrations were largely overestimated at the SMEAR-II site (likely because of the overstated isoprene emissions) and especially during periods characterized by high temperatures and intensive photochemical activity (referred to as "heat wave" episode). Particle mass yield from isoprene biogenic compounds is lower compared to monoterpenes and recent studies have shown that isoprene can effectively scavenge $^{\cdot}OH$ radicals, preventing their reactions against other terpenoids therefore limiting the formation of biogenic aerosol particles and the total organic mass (McFiggans et al., 2019).

Figure 14 reports the daytime relative changes in α-pinene, O_3 and BSOA concentrations between the two simulations performed with and without isoprene emissions across all Europe. Inhibiting isoprene emissions resulted in a non-negligible increase in the BSOA mass concentrations over larger areas of northern part of the domain. In most of the areas, the BSOA mass increased by about 10 % with maximum increases at around 25 %. Conversely, α-pinene air concentrations were homogenously reduced all over the domain (Figure 14). The relative reductions (over land) were on the order of 10 to 20 %. As isoprene emissions are excluded from the modelling system, more α-pinene of biogenic origin can effectively react towards available radicals, i.e. ·OH radicals, and, owing to its higher mass yield compared to isoprene, effectively increase the production efficiency of BSOA. This process is likely favored by the large pool of α-pinene emissions available over the boreal forest regions (and by the lower temperatures compared to continental and southern Europe) which favors the transition of oxidized gases in the particle phase. Figure 14 also reports the relative changes in O_3 concentrations between the two simulations performed with and without isoprene emissions which were predicted to be very mild over the northern Europe and larger over continental and southern Europe because of enhanced photochemical activities and large availability of isoprene emissions in the southern regions of the domain. Formation of O_3 is driven by the availability of both NO_x and VOCs emissions, with the investigated area, SMEAR-II, clearly belonging to a NO_x-limited regime. As reported in the Figure 15, the model is capable to reproduce the diurnal variation and absolute values (ppb) of O_3 very well (mean bias of -0.1 ppb and 0.3 ppb for O_3 and NO_x, respectively, Table 4), whereas NOx concentrations were overestimated during nighttime periods, a behavior that was also confirmed by an additional evaluation against NO_x and O_3 measurements retrieved across whole Europe from the Air Quality e-Reporting database (https://www.eea.europa.eu/en) (Figure S3 and Table S4). Additionally, both model and measurements data, did not show a substantial local production of O_3 concentrations, i.e., both model and observational O_3 values increased from about 25 to about 30 ppb. This suggests that a large fraction of the O_3 measured at the SMEAR-II

sites is of long-range origin, therefore explaining the relative low changes in its concentrations between the two scenarios in the northern regions, as also reported by previous studies (Curci et al., 2009).

4 Conclusions

We presented a modeling evaluation study aiming at evaluating the formation of biogenic secondary organic aerosol over the Finnish Boreal Forest with the WRF-CHIMEREv2020r2 model. We investigated the formation of BSOA using different aging schemes to treat the second-generation oxidation product of BSOA, also referred to as chemical aging, as currently available from literature. Results were evaluated against high-resolution organic aerosol (OA) measurements performed with an aerosol chemical speciation monitor (ACSM) at the SMEAR-II site, an area largely affected by biogenic emissions. We used parallel measurements of biogenic gas-phase precursors (i.e., isoprene and monoterpenes) to investigate the model performance with respect to the BSOA precursors which offers a proper framework to evaluate Chemical Transport Model (CTM) simulations to a greater level of details. Additionally, we evaluate the model's response to changes in isoprene emissions and the impact of different chemical schemes on the predicted Cloud Liquid Water Content (clwc).

The meteorological evaluation of standard parameters affecting the formation and transportation of BSOA was found to be satisfactory reproduced throughout the whole simulated period, underlying the capability of the WRF model to properly reproduce the meteorological regimes of the summer of 2019 at a 10 kilometers grid resolution.

The model could well reproduce the diurnal variation of the OA mass as measured at the SMEAR-II site. As expected, aging processes of BSOA largely increased the BSOA mass, yielding reasonable model performance, both in term of the total OA mass as well as in terms of sources contribution (i.e. POA, ASOA and BSOA), for schemes that account for aging of BSOA as proposed in previous study (Bergström et al., 2012). On the other side, the analysis of the model size distribution indicated a large overestimation for particles below about 100 nanometers and an underestimation for particles in the larger diameter sizes. We attributed such compensating effect to 1) a lack of an explicit treatment of organic compounds in the LVOC and ELVOC range, which can effectively condense on smaller particles and promote their growth to larger particles size, and to a lesser extent 2) to the lack of the kelvin effect in the model calculation. Overall, those results stressed once more the need to proper represent the volatility distribution in CTM application, and more work is needed towards this direction, particularly on the volatility distribution of BSOA and on the implementation of physical processes affecting the evolution of the size distribution (e.g., inclusion of organic gases in the very low volatility ranges).

Additionally, the analysis of biogenic gas-phase precursors indicated that the model largely overestimated isoprene emissions likely because of overstated emissions in the MEGAN emission model, as already presented in various application of the MEGAN model at European scale. There is still a need to further reduce the uncertainties in the current estimation of biogenic fluxes (especially at northern latitudes) one of the key parameters influencing the formation of BSOA in CTMs. An additional sensitive test indicated that an overestimation could potentially reduce the production of BSOA by scavenging away $^{\cdot}OH$ radicals that would have been available to react against α-pinene compounds which have higher SOA yields.

Finally, our model results indicated an increase in the cloud liquid water content when aging of BSOA are accounted for, likely because of the increased number of aerosols particles acting as cloud condensation nuclei (CCN), as recently also suggested

by measurements studies conducted at the SMEAR-II site. These preliminary results reported here should be corroborated in a greater level of details by a more detailed modeling studying spanning multiple years (i.e., trend-analysis).

Overall, the model evaluation presented here indicated once more the importance of properly characterize both biogenic emissions fluxes and chemical scheme parameterization to correctly predict the formation of BSOA and its size distribution. As climate continues to warm, biogenic emissions could become an increasingly important contributor to the total OA pool, and model predictions could largely varies depending, also, on the level of confidence of emission strength and chemical parameterization.

Code availability

The WRF-CHIMERE model is freely available at https://www.lmd.polytechnique.fr/chimere/ (registration required).

Data availability.

Biogenic emissions input data, boundary conditions, model output data, observational data and the source code of WRF-CHIMERE used here are all available at the following repository https://doi.org/10.5281/zenodo.8055256.
The input data used for the simulations are also available at https://www.lmd.polytechnique.fr/chimere/2020_getcode.php. The full CAM anthropogenic emission can be downloaded at https://eccad3.sedoo.fr/catalogue, dataset name: CAMS-GLOB-ANT. Measurements data from the SMEAR-II station can additionally be downloaded at https://smear.avaa.csc.fi/download. The ACSM NR-PM_1 OA concentration data are available on the EBAS database under the EMEP ACTRIS framework (http://ebas.nilu.no/).

Acknowledgment

This work was supported by the European Research Council via the project CHAPAs (No. 850614) and by the Academy of Finland (Nos. 311932, 307537, 334792, 337549). Model simulations were performed "online" with the meteorological model on the mahti supercomputer of the Finnish IT center for science (CSC) using 1 computing node for the European grid, and 4 computing nodes for the high-resolution domain. We would like to thank Juha Lento for his continuous support at the Finnish IT center for science (CSC). We are also thankful to Liine Heikkinen and Mikael Ehn for their inputs on the manuscript.

Author contributions

G. C. designed and led the work in collaboration with F.B., performed the WRF-CHIMERE simulations, and wrote the paper. A.C. provided technical support during the operational phases of the WRF-CHIMERE model, recommendations on the model set-up and errors handling support. S. T. performed the data analysis of the model data in collaboration with B.V.. T.P. provided technical support in handling the instrumentation datasets. All co-authors review commented and supported the interpretation of the results presented in the paper.

Conflicts of interest

The authors declare that they have no conflict of interest.

References

Abdul-Razzak, H., 2002. A parameterization of aerosol activation 3. Sectional representation. J. Geophys. Res. 107, 4026. https://doi.org/10.1029/2001JD000483

Aksoyoglu, S., Keller, J., Barmpadimos, I., Oderbolz, D., Lanz, V.A., Prévôt, A.S.H., Baltensperger, U., 2011. Aerosol modelling in Europe with a focus on Switzerland during summer and winter episodes. Atmos. Chem. Phys. 11, 7355–7373. https://doi.org/10.5194/acp-11-7355-2011

Bergström, R., Denier van der Gon, H.A.C., Prévôt, A.S.H., Yttri, K.E., Simpson, D., 2012. Modelling of organic aerosols over Europe (2002–2007) using a volatility basis set (VBS) framework: application of different assumptions regarding the formation of secondary organic aerosol. Atmos. Chem. Phys. 12, 8499–8527. https://doi.org/10.5194/acp-12-8499-2012

Bergström, R., Hallquist, M., Simpson, D., Wildt, J., Mentel, T.F., 2014. Biotic stress: a significant contributor to organic aerosol in Europe? Atmos. Chem. Phys. 14, 13643–13660. https://doi.org/10.5194/acp-14-13643-2014

Bessagnet, B., Menut, L., Colette, A., Couvidat, F., Dan, M., Mailler, S., Létinois, L., Pont, V., Rouïl, L., 2017. An Evaluation of the CHIMERE Chemistry Transport Model to Simulate Dust Outbreaks across the Northern Hemisphere in March 2014. Atmosphere 8, 251. https://doi.org/10.3390/atmos8120251

Bessagnet, B., Menut, L., Curci, G., Hodzic, A., Guillaume, B., Liousse, C., Moukhtar, S., Pun, B., Seigneur, C., Schulz, M., 2008. Regional modeling of carbonaceous aerosols over Europe—focus on secondary organic aerosols. J Atmos Chem 61, 175–202. https://doi.org/10.1007/s10874-009-9129-2

Bessagnet, B., Pirovano, G., Mircea, M., Cuvelier, C., Aulinger, A., Calori, G., Ciarelli, G., Manders, A., Stern, R., Tsyro, S., García Vivanco, M., Thunis, P., Pay, M.-T., Colette, A., Couvidat, F., Meleux, F., Rouïl, L., Ung, A., Aksoyoglu, S., Baldasano, J.M., Bieser, J., Briganti, G., Cappelletti, A., D'Isidoro, M., Finardi, S., Kranenburg, R., Silibello, C., Carnevale, C., Aas, W., Dupont, J.-C., Fagerli, H., Gonzalez, L., Menut, L., Prévôt, A.S.H., Roberts, P., White, L., 2016. Presentation of the EURODELTA III intercomparison exercise – evaluation of the chemistry transport models' performance on criteria pollutants and joint analysis with meteorology. Atmos. Chem. Phys. 16, 12667–12701. https://doi.org/10.5194/acp-16-12667-2016

Bianchi, F., Junninen, H., Bigi, A., Sinclair, V.A., Dada, L., Hoyle, C.R., Zha, Q., Yao, L., Ahonen, L.R., Bonasoni, P., Buenrostro Mazon, S., Hutterli, M., Laj, P., Lehtipalo, K., Kangasluoma, J., Kerminen, V.-M., Kontkanen, J., Marinoni, A., Mirme, S., Molteni, U., Petäjä, T., Riva, M., Rose, C., Sellegri, K., Yan, C., Worsnop, D.R., Kulmala, M., Baltensperger, U., Dommen, J., 2021. Biogenic particles formed in the Himalaya as an important source of free tropospheric aerosols. Nat. Geosci. 14, 4–9. https://doi.org/10.1038/s41561-020-00661-5

Bianchi, F., Kurtén, T., Riva, M., Mohr, C., Rissanen, M.P., Roldin, P., Berndt, T., Crounse, J.D., Wennberg, P.O., Mentel, T.F., Wildt, J., Junninen, H., Jokinen, T., Kulmala, M., Worsnop, D.R., Thornton, J.A., Donahue, N., Kjaergaard, H.G., Ehn, M., 2019. Highly Oxygenated Organic Molecules (HOM) from Gas-Phase Autoxidation Involving Peroxy Radicals: A Key Contributor to Atmospheric Aerosol. Chem. Rev. 119, 3472–3509. https://doi.org/10.1021/acs.chemrev.8b00395

Boy, M., Zhou, P., Kurtén, T., Chen, D., Xavier, C., Clusius, P., Roldin, P., Baykara, M., Pichelstorfer, L., Foreback, B., Bäck, J., Petäjä, T., Makkonen, R., Kerminen, V.-M., Pihlatie, M., Aalto, J., Kulmala, M., 2022. Positive feedback mechanism between biogenic volatile organic compounds and the methane lifetime in future climates. npj Clim Atmos Sci 5, 72. https://doi.org/10.1038/s41612-022-00292-0

Briant, R., Tuccella, P., Deroubaix, A., Khvorostyanov, D., Menut, L., Mailler, S., Turquety, S., 2017. Aerosol–radiation interaction modelling using online coupling between the WRF 3.7.1 meteorological model and the CHIMERE 2016 chemistry-transport model, through the OASIS3-MCT coupler. Geoscientific Model Development 10, 927–944. https://doi.org/10.5194/gmd-10-927-2017

Chapman, E.G., Gustafson, W.I., Easter, R.C., Barnard, J.C., Ghan, S.J., Pekour, M.S., Fast, J.D., 2009. Coupling aerosol-cloud-radiative processes in the WRF-Chem model: Investigating the radiative impact of elevated point sources. Atmos. Chem. Phys. 9, 945–964. https://doi.org/10.5194/acp-9-945-2009

Chen, F., Dudhia, J., 2001. Coupling an Advanced Land Surface–Hydrology Model with the Penn State–NCAR MM5 Modeling System. Part I: Model Implementation and Sensitivity. Monthly Weather Review 129, 569–585. https://doi.org/10.1175/1520-0493(2001)129<0569:CAALSH>2.0.CO;2

Chin, M., Ginoux, P., Kinne, S., Torres, O., Holben, B.N., Duncan, B.N., Martin, R.V., Logan, J.A., Higurashi, A., Nakajima, T., 2002. Tropospheric Aerosol Optical Thickness from the GOCART Model and Comparisons with Satellite and Sun Photometer Measurements. Journal of the Atmospheric Sciences 59, 461–483. https://doi.org/10.1175/1520-0469(2002)059<0461:TAOTFT>2.0.CO;2

Cholakian, A., Beekmann, M., Colette, A., Coll, I., Siour, G., Sciare, J., Marchand, N., Couvidat, F., Pey, J., Gros, V., Sauvage, S., Michoud, V., Sellegri, K., Colomb, A., Sartelet, K., Langley DeWitt, H., Elser, M., Prévot, A.S.H., Szidat, S., Dulac, F., 2018. Simulation of fine organic aerosols in the western Mediterranean area during the ChArMEx 2013 summer campaign. Atmos. Chem. Phys. 18, 7287–7312. https://doi.org/10.5194/acp-18-7287-2018

Cholakian, A., Beekmann, M., Colette, A., Coll, I., Siour, G., Sciare, J., Marchand, N., Couvidat, F., Pey, J., Gros, V., Sauvage, S., Michoud, V., Sellegri, K., Colomb, A., Sartelet, K., Langley DeWitt, H., Elser, M., Prévot, A.S.H., Szidat, S., Dulac, F., 2017. Simulation of fine organic aerosols in the western Mediterranean area during the ChArMEx 2013 summer campaign. Atmos. Chem. Phys. Discuss. 2017, 1–45. https://doi.org/10.5194/acp-2017-697

Cholakian, A., Beekmann, M., Siour, G., Coll, I., Cirtog, M., Ormeno, E., Flaud, P.-M., Perraudin, E., Villenave, E., 2022. Simulation of organic aerosol, its precursors and related oxidants in the Landes pine forest in south-western France: Need to account for domain specific land-use and physical conditions (preprint). Aerosols/Atmospheric Modelling/Troposphere/Chemistry (chemical composition and reactions). https://doi.org/10.5194/acp-2022-697

Ciarelli, G., Aksoyoglu, S., Crippa, M., Jimenez, J.-L., Nemitz, E., Sellegri, K., Äijälä, M., Carbone, S., Mohr, C., O'Dowd, C., Poulain, L., Baltensperger, U., Prévôt, A.S.H., 2016. Evaluation of European air quality modelled by CAMx including the volatility basis set scheme. Atmos. Chem. Phys. 16, 10313–10332. https://doi.org/10.5194/acp-16-10313-2016

Ciarelli, G., Theobald, M.R., Vivanco, M.G., Beekmann, M., Aas, W., Andersson, C., Bergström, R., Manders-Groot, A., Couvidat, F., Mircea, M., Tsyro, S., Fagerli, H., Mar, K., Raffort, V., Roustan, Y., Pay, M.-T., Schaap, M., Kranenburg, R., Adani, M., Briganti, G., Cappelletti, A., D'Isidoro, M., Cuvelier, C., Cholakian, A., Bessagnet, B., Wind, P., Colette, A., 2019. Trends of inorganic and organic aerosols and precursor gases in Europe: insights from the EURODELTA multi-model experiment over the 1990–2010 period. Geosci. Model Dev. 12, 4923–4954. https://doi.org/10.5194/gmd-12-4923-2019

Curci, G., Beekmann, M., Vautard, R., Smiatek, G., Steinbrecher, R., Theloke, J., Friedrich, R., 2009. Modelling study of the impact of isoprene and terpene biogenic emissions on European ozone levels. Atmospheric Environment, Natural and Biogenic Emissions of Environmentally Relevant Atmospheric Trace Constituents in Europe 43, 1444–1455. https://doi.org/10.1016/j.atmosenv.2008.02.070

Debry, E., Fahey, K., Sartelet, K., Sportisse, B., Tombette, M., 2007. Technical Note: A new SIze REsolved Aerosol Model (SIREAM). Atmospheric Chemistry and Physics 7, 1537–1547. https://doi.org/10.5194/acp-7-1537-2007

Derognat, C., 2003. Effect of biogenic volatile organic compound emissions on tropospheric chemistry during the Atmospheric Pollution Over the Paris Area (ESQUIF) campaign in the Ile-de-France region. J. Geophys. Res. 108, 8560. https://doi.org/10.1029/2001JD001421

Donahue, N.M., Epstein, S.A., Pandis, S.N., Robinson, A.L., 2011. A two-dimensional volatility basis set: 1. organic-aerosol mixing thermodynamics. Atmos. Chem. Phys. 11, 3303–3318. https://doi.org/10.5194/acp-11-3303-2011

Donahue, Neil M., Henry, K.M., Mentel, T.F., Kiendler-Scharr, A., Spindler, C., Bohn, B., Brauers, T., Dorn, H.P., Fuchs, H., Tillmann, R., Wahner, A., Saathoff, H., Naumann, K.-H., Möhler, O., Leisner, T., Müller, L., Reinnig, M.-C., Hoffmann, T., Salo, K., Hallquist, M., Frosch, M., Bilde, M., Tritscher, T., Barmet, P., Praplan, A.P., DeCarlo, P.F., Dommen, J., Prévôt, A.S.H., Baltensperger, U., 2012. Aging of biogenic secondary organic aerosol via gas-phase OH radical reactions. Proc. Natl. Acad. Sci. U.S.A. 109, 13503–13508. https://doi.org/10.1073/pnas.1115186109

Donahue, N. M., Kroll, J.H., Pandis, S.N., Robinson, A.L., 2012. A two-dimensional volatility basis set – Part 2: Diagnostics of organic-aerosol evolution. Atmos. Chem. Phys. 12, 615–634. https://doi.org/10.5194/acp-12-615-2012

Guenther, A., 1997. SEASONAL AND SPATIAL VARIATIONS IN NATURAL VOLATILE ORGANIC COMPOUND EMISSIONS. Ecological Applications 7, 34–45. https://doi.org/10.1890/1051-0761(1997)007[0034:SASVIN]2.0.CO;2

Guenther, A., Karl, T., Harley, P., Wiedinmyer, C., Palmer, P.I., Geron, C., 2006. Estimates of global terrestrial isoprene emissions using MEGAN (Model of Emissions of Gases and Aerosols from Nature). Atmospheric Chemistry and Physics 6, 3181–3210. https://doi.org/10.5194/acp-6-3181-2006

Guenther, A.B., Jiang, X., Heald, C.L., Sakulyanontvittaya, T., Duhl, T., Emmons, L.K., Wang, X., 2012. The Model of Emissions of Gases and Aerosols from Nature version 2.1 (MEGAN2.1): an extended and updated framework for modeling biogenic emissions. Geosci. Model Dev. 5, 1471–1492. https://doi.org/10.5194/gmd-5-1471-2012

Hari, P., Kulmala, M., 2005. Station for Measuring Ecosystem–Atmosphere Relations (SMEAR II). Boreal Env. Res. 10., 315-322.

Hauglustaine, D.A., Balkanski, Y., Schulz, M., 2014. A global model simulation of present and future nitrate aerosols and their direct radiative forcing of climate. Atmospheric Chemistry and Physics 14, 11031–11063. https://doi.org/10.5194/acp-14-11031-2014

Heikkinen, L., Äijälä, M., Daellenbach, K.R., Chen, G., Garmash, O., Aliaga, D., Graeffe, F., Räty, M., Luoma, K., Aalto, P., Kulmala, M., Petäjä, T., Worsnop, D., Ehn, M., 2021. Eight years of sub-micrometre organic aerosol composition data from the boreal forest characterized using a machine-learning approach. Atmospheric Chemistry and Physics 21, 10081–10109. https://doi.org/10.5194/acp-21-10081-2021

Hellén, H., Praplan, A.P., Tykkä, T., Ylivinkka, I., Vakkari, V., Bäck, J., Petäjä, T., Kulmala, M., Hakola, H., 2018. Long-term measurements of volatile organic compounds highlight the importance of sesquiterpenes for the atmospheric chemistry of a boreal forest. Atmos. Chem. Phys. 18, 13839–13863. https://doi.org/10.5194/acp-18-13839-2018

Hodzic, A., Jimenez, J.L., 2011. Modeling anthropogenically controlled secondary organic aerosols in a megacity: a simplified framework for global and climate models. Geosci. Model Dev. 4, 901–917. https://doi.org/10.5194/gmd-4-901-2011

Hodzic, A., Jimenez, J.L., Madronich, S., Aiken, A.C., Bessagnet, B., Curci, G., Fast, J., Lamarque, J.-F., Onasch, T.B., Roux, G., Schauer, J.J., Stone, E.A., Ulbrich, I.M., 2009. Modeling organic aerosols during MILAGRO: importance of biogenic secondary organic aerosols. Atmos. Chem. Phys. 9, 6949–6981. https://doi.org/10.5194/acp-9-6949-2009

Hong, S.-Y., Dudhia, J., Chen, S.-H., 2004. A Revised Approach to Ice Microphysical Processes for the Bulk Parameterization of Clouds and Precipitation. Monthly Weather Review 132, 103–120. https://doi.org/10.1175/1520-0493(2004)132<0103:ARATIM>2.0.CO;2

Jacobson, M.Z., 2005. Fundamentals of Atmospheric Modeling, 2nd ed. Cambridge University Press. https://doi.org/10.1017/CBO9781139165389

Janjic, Z.I., 2003. A nonhydrostatic model based on a new approach. Meteorol Atmos Phys 82, 271–285. https://doi.org/10.1007/s00703-001-0587-6

Jiang, J., Aksoyoglu, S., Ciarelli, G., Oikonomakis, E., El-Haddad, I., Canonaco, F., O'Dowd, C., Ovadnevaite, J., Minguillón, M.C., Baltensperger, U., Prévôt, A.S.H., 2019a. Effects of two different biogenic emission models on modelled ozone and aerosol concentrations in Europe. Atmos. Chem. Phys. 19, 3747–3768. https://doi.org/10.5194/acp-19-3747-2019

Jiang, J., Aksoyoglu, S., El-Haddad, I., Ciarelli, G., Denier van der Gon, H.A.C., Canonaco, F., Gilardoni, S., Paglione, M., Minguillón, M.C., Favez, O., Zhang, Y., Marchand, N., Hao, L., Virtanen, A., Florou, K., O'Dowd, C., Ovadnevaite, J., Baltensperger, U., Prévôt, A.S.H., 2019b. Sources of organic aerosols in Europe: a modeling study using CAMx with modified volatility basis set scheme. Atmos. Chem. Phys. 19, 15247–15270. https://doi.org/10.5194/acp-19-15247-2019

Kulmala, M., Laaksonen, A., Pirjola, L., 1998. Parameterizations for sulfuric acid/water nucleation rates. J. Geophys. Res. 103, 8301–8307. https://doi.org/10.1029/97JD03718

Lane, T.E., Donahue, N.M., Pandis, S.N., 2008. Simulating secondary organic aerosol formation using the volatility basis-set approach in a chemical transport model. Atmospheric Environment 42, 7439–7451. https://doi.org/10.1016/j.atmosenv.2008.06.026

Lindfors, V., Laurila, T., 2000. Biogenic volatile organic compound (VOC) emissions from forests in Finland. Boreal Env. Res. 5, 95–113.

Mailler, S., Menut, L., Khvorostyanov, D., Valari, M., Couvidat, F., Siour, G., Turquety, S., Briant, R., Tuccella, P., Bessagnet, B., Colette, A., Létinois, L., Markakis, K., Meleux, F., 2017. CHIMERE-2017: from urban to hemispheric chemistry-transport modeling. Geosci. Model Dev. 10, 2397–2423. https://doi.org/10.5194/gmd-10-2397-2017

McFiggans, G., Mentel, T.F., Wildt, J., Pullinen, I., Kang, S., Kleist, E., Schmitt, S., Springer, M., Tillmann, R., Wu, C., Zhao, D., Hallquist, M., Faxon, C., Le Breton, M., Hallquist, Å.M., Simpson, D., Bergström, R., Jenkin, M.E., Ehn, M., Thornton, J.A., Alfarra, M.R., Bannan, T.J., Percival, C.J., Priestley, M., Topping, D., Kiendler-Scharr, A., 2019. Secondary organic aerosol reduced by mixture of atmospheric vapours. Nature 565, 587–593. https://doi.org/10.1038/s41586-018-0871-y

Menut, L., Bessagnet, B., Briant, R., Cholakian, A., Couvidat, F., Mailler, S., Pennel, R., Siour, G., Tuccella, P., Turquety, S., Valari, M., 2021. The CHIMERE v2020r1 online chemistry-transport model (preprint). Atmospheric sciences. https://doi.org/10.5194/gmd-2021-96

Mlawer, E.J., Taubman, S.J., Brown, P.D., Iacono, M.J., Clough, S.A., 1997. Radiative transfer for inhomogeneous atmospheres: RRTM, a validated correlated-k model for the longwave. Journal of Geophysical Research: Atmospheres 102, 16663–16682. https://doi.org/10.1029/97JD00237

Murphy, B.N., Pandis, S.N., 2009. Simulating the Formation of Semivolatile Primary and Secondary Organic Aerosol in a Regional Chemical Transport Model. Environ. Sci. Technol. 43, 4722–4728. https://doi.org/10.1021/es803168a

Nenes, A., Pandis, S.N., Pilinis, C., 1998. ISORROPIA: A New Thermodynamic Equilibrium Model for Multiphase Multicomponent Inorganic Aerosols. Aquatic Geochemistry 4, 123–152. https://doi.org/10.1023/A:1009604003981

Oderbolz, D.C., Aksoyoglu, S., Keller, J., Barmpadimos, I., Steinbrecher, R., Skjøth, C.A., Plaß-Dülmer, C., Prévôt, A.S.H., 2013. A comprehensive emission inventory of biogenic volatile organic compounds in Europe: improved seasonality and land-cover. Atmos. Chem. Phys. 13, 1689–1712. https://doi.org/10.5194/acp-13-1689-2013

Odum, J.R., Hoffmann, T., Bowman, F., Collins, D., Flagan, R.C., Seinfeld, J.H., 1996. Gas/Particle Partitioning and Secondary Organic Aerosol Yields. Environ. Sci. Technol. 30, 2580–2585. https://doi.org/10.1021/es950943+

Peñuelas, J., Asensio, D., Tholl, D., Wenke, K., Rosenkranz, M., Piechulla, B., Schnitzler, J.P., 2014. Biogenic volatile emissions from the soil: Biogenic volatile emissions from the soil. Plant Cell Environ 37, 1866–1891. https://doi.org/10.1111/pce.12340

Rantala, P., Aalto, J., Taipale, R., Ruuskanen, T.M., Rinne, J., 2015. Annual cycle of volatile organic compound exchange between a boreal pine forest and the atmosphere. Biogeosciences 12, 5753–5770. https://doi.org/10.5194/bg-12-5753-2015

Robinson, A.L., Donahue, N.M., Shrivastava, M.K., Weitkamp, E.A., Sage, A.M., Grieshop, A.P., Lane, T.E., Pierce, J.R., Pandis, S.N., 2007. Rethinking Organic Aerosols: Semivolatile Emissions and Photochemical Aging. Science 315, 1259–1262. https://doi.org/10.1126/science.1133061

Seinfeld, J.H., Pandis, S.N., 2012. Atmospheric Chemistry and Physics: From Air Pollution to Climate Change. Wiley.

Shrivastava, M., Easter, R.C., Liu, X., Zelenyuk, A., Singh, B., Zhang, K., Ma, P.-L., Chand, D., Ghan, S., Jimenez, J.L., Zhang, Q., Fast, J., Rasch, P.J., Tiitta, P., 2015. Global transformation and fate of SOA: Implications of low-volatility SOA and gas-phase fragmentation reactions: Global Modeling of SOA. J. Geophys. Res. Atmos. 120, 4169–4195. https://doi.org/10.1002/2014JD022563

Simpson, D., Benedictow, A., Berge, H., Bergström, R., Emberson, L.D., Fagerli, H., Flechard, C.R., Hayman, G.D., Gauss, M., Jonson, J.E., Jenkin, M.E., Nyíri, A., Richter, C., Semeena, V.S., Tsyro, S., Tuovinen, J.-P., Valdebenito, Á., Wind, P., 2012. The EMEP MSC-W chemical transport model – technical description. Atmos. Chem. Phys. 12, 7825–7865. https://doi.org/10.5194/acp-12-7825-2012

Sinclair, V.A., Ritvanen, J., Urbancic, G., Statnaia, I., Batrak, Y., Moisseev, D., Kurppa, M., 2022. Boundary-layer height and surface stability at Hyytiälä, Finland, in ERA5 and observations. Atmos. Meas. Tech. 15, 3075–3103. https://doi.org/10.5194/amt-15-3075-2022

Sindelarova, K., Granier, C., Bouarar, I., Guenther, A., Tilmes, S., Stavrakou, T., Müller, J.-F., Kuhn, U., Stefani, P., Knorr, W., 2014. Global data set of biogenic VOC emissions calculated by the MEGAN model over the last 30 years. Atmos. Chem. Phys. 14, 9317–9341. https://doi.org/10.5194/acp-14-9317-2014

Skamarock, W., Klemp, J., Dudhia, J., Gill, D., Barker, D., Wang, W., Huang, X.Y., Duda, M., 2008. A Description of the Advanced Research WRF Version 3. UCAR/NCAR. https://doi.org/10.5065/D68S4MVH

Solazzo, E., Hogrefe, C., Colette, A., Garcia-Vivanco, M., Galmarini, S., 2017. Advanced error diagnostics of the CMAQ and Chimere modelling systems within the AQMEII3 model evaluation framework. Atmospheric Chemistry and Physics 17, 10435–10465. https://doi.org/10.5194/acp-17-10435-2017

Sousa, P.M., Barriopedro, D., Ramos, A.M., García-Herrera, R., Espírito-Santo, F., Trigo, R.M., 2019. Saharan air intrusions as a relevant mechanism for Iberian heatwaves: The record breaking events of August 2018 and June 2019. Weather and Climate Extremes 26, 100224. https://doi.org/10.1016/j.wace.2019.100224

Theobald, M.R., Vivanco, M.G., Aas, W., Andersson, C., Ciarelli, G., Couvidat, F., Cuvelier, K., Manders, A., Mircea, M., Pay, M.-T., Tsyro, S., Adani, M., Bergström, R., Bessagnet, B., Briganti, G., Cappelletti, A., D'Isidoro, M., Fagerli, H., Mar, K., Otero, N., Raffort, V., Roustan, Y., Schaap, M., Wind, P., Colette, A., 2019. An evaluation of European

nitrogen and sulfur wet deposition and their trends estimated by six chemistry transport models for the period 1990–2010. Atmos. Chem. Phys. 19, 379–405. https://doi.org/10.5194/acp-19-379-2019

Tomczyk, A., Półrolniczak, M., Bednorz, E., 2017. Circulation Conditions' Effect on the Occurrence of Heat Waves in Western and Southwestern Europe. Atmosphere 8, 31. https://doi.org/10.3390/atmos8020031

Tsigaridis, K., Daskalakis, N., Kanakidou, M., Adams, P.J., Artaxo, P., Bahadur, R., Balkanski, Y., Bauer, S.E., Bellouin, N., Benedetti, A., Bergman, T., Berntsen, T.K., Beukes, J.P., Bian, H., Carslaw, K.S., Chin, M., Curci, G., Diehl, T., Easter, R.C., Ghan, S.J., Gong, S.L., Hodzic, A., Hoyle, C.R., Iversen, T., Jathar, S., Jimenez, J.L., Kaiser, J.W., Kirkevåg, A., Koch, D., Kokkola, H., Lee, Y.H., Lin, G., Liu, X., Luo, G., Ma, X., Mann, G.W., Mihalopoulos, N., Morcrette, J.-J., Müller, J.-F., Myhre, G., Myriokefalitakis, S., Ng, N.L., O'Donnell, D., Penner, J.E., Pozzoli, L., Pringle, K.J., Russell, L.M., Schulz, M., Sciare, J., Seland, Ø., Shindell, D.T., Sillman, S., Skeie, R.B., Spracklen, D., Stavrakou, T., Steenrod, S.D., Takemura, T., Tiitta, P., Tilmes, S., Tost, H., van Noije, T., van Zyl, P.G., von Salzen, K., Yu, F., Wang, Z., Wang, Z., Zaveri, R.A., Zhang, H., Zhang, K., Zhang, Q., Zhang, X., 2014. The AeroCom evaluation and intercomparison of organic aerosol in global models. Atmos. Chem. Phys. 14, 10845–10895. https://doi.org/10.5194/acp-14-10845-2014

Tsimpidi, A.P., Karydis, V.A., Zavala, M., Lei, W., Molina, L., Ulbrich, I.M., Jimenez, J.L., Pandis, S.N., 2010. Evaluation of the volatility basis-set approach for the simulation of organic aerosol formation in the Mexico City metropolitan area. Atmos. Chem. Phys. 22.

Tuccella, P., Menut, L., Briant, R., Deroubaix, A., Khvorostyanov, D., Mailler, S., Siour, G., Turquety, S., 2019. Implementation of Aerosol-Cloud Interaction within WRF-CHIMERE Online Coupled Model: Evaluation and Investigation of the Indirect Radiative Effect from Anthropogenic Emission Reduction on the Benelux Union. Atmosphere 10, 20. https://doi.org/10.3390/atmos10010020

Vestenius, M., Hopke, P.K., Lehtipalo, K., Petäjä, T., Hakola, H., Hellén, H., 2021. Assessing volatile organic compound sources in a boreal forest using positive matrix factorization (PMF). Atmospheric Environment 259, 118503. https://doi.org/10.1016/j.atmosenv.2021.118503

Villiers, M.P., 2020. Europe extreme heat 22–26 July 2019: was it caused by subsidence or advection? Weather 75, 228–235. https://doi.org/10.1002/wea.3717

Xu, R., Thornton, J.A., Lee, B.H., Zhang, Y., Jaeglé, L., Lopez-Hilfiker, F.D., Rantala, P., Petäjä, T., 2022. Global simulations of monoterpene-derived peroxy radical fates and the distributions of highly oxygenated organic molecules (HOMs) and accretion products. Atmos. Chem. Phys. 22, 5477–5494. https://doi.org/10.5194/acp-22-5477-2022

Yli-Juuti, T., Mielonen, T., Heikkinen, L., Arola, A., Ehn, M., Isokääntä, S., Keskinen, H.-M., Kulmala, M., Laakso, A., Lipponen, A., Luoma, K., Mikkonen, S., Nieminen, T., Paasonen, P., Petäjä, T., Romakkaniemi, S., Tonttila, J., Kokkola, H., Virtanen, A., 2021. Significance of the organic aerosol driven climate feedback in the boreal area. Nat Commun 12, 5637. https://doi.org/10.1038/s41467-021-25850-7

Zhang, Q.J., Beekmann, M., Drewnick, F., Freutel, F., Schneider, J., Crippa, M., Prevot, A.S.H., Baltensperger, U., Poulain, L., Wiedensohler, A., Sciare, J., Gros, V., Borbon, A., Colomb, A., Michoud, V., Doussin, J.-F., Denier van der Gon, H.A.C., Haeffelin, M., Dupont, J.-C., Siour, G., Petetin, H., Bessagnet, B., Pandis, S.N., Hodzic, A., Sanchez, O., Honoré, C., Perrussel, O., 2013. Formation of organic aerosol in the Paris region during the MEGAPOLI summer campaign: evaluation of the volatility-basis-set approach within the CHIMERE model. Atmos. Chem. Phys. 13, 5767–5790. https://doi.org/10.5194/acp-13-5767-2013

Zhang, Q.J., Beekmann, M., Freney, E., Sellegri, K., Pichon, J.M., Schwarzenboeck, A., Colomb, A., Bourrianne, T., Michoud, V., Borbon, A., 2015. Formation of secondary organic aerosol in the Paris pollution plume and its impact on surrounding regions. Atmos. Chem. Phys. 15, 13973–13992. https://doi.org/10.5194/acp-15-13973-2015

Zhao, T., Mao, J., Ayazpour, Z., González Abad, G., Nowlan, C., Zheng, Y., 2023. Interannual variability of summertime formaldehyde (HCHO) vertical column density and its main drivers in northern high latitudes (preprint). Gases/Atmospheric Modelling and Data Analysis/Troposphere/Chemistry (chemical composition and reactions). https://doi.org/10.5194/egusphere-2023-1431

Figures and Tables

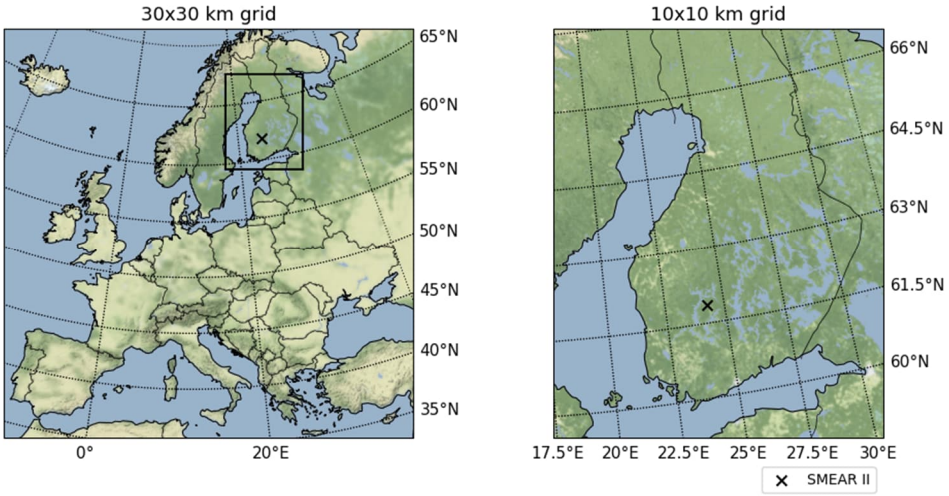

Figure 1: The two model domains: the European grid (left) with a cell size of ~ 30 x 30 km, and the nested grid (right) with a cell size of ~ 10 x 10 km (right). The black square on the European grid (left) indicates the position of the nesting. The black cross denotes the location of the SMEAR-II station.

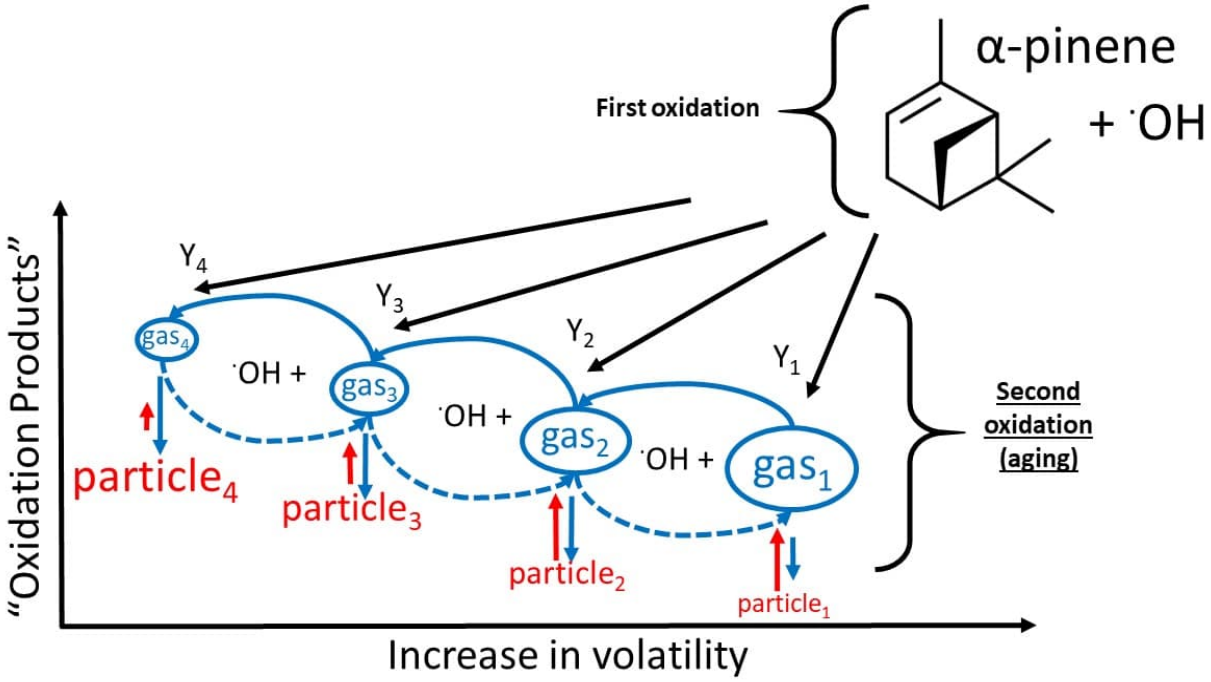

Figure 2: Schematic of the oxidation scheme of biogenic precursors as implemented in the VBS scheme of CHIMERE (here reported specifically for the $C_{10}H_{16}$ parent precursor). The black arrows represent the distribution kernel of the first oxidation products into the four volatility bins (Y_1…Y_4). The blue curved arrows represent the secondary oxidation processes, i.e., aging, along the four volatility bins, each of which decreases the volatility by one order of magnitude. The text font size represents the tendency of both particles and gas-phase organic material (OM) to transition in the one or the other phase (i.e., larger font size indicates a stronger affinity towards that phase, and vice versa). The dashed curved arrows represent the fragmentation process (also available in CHIMERE, but not currently used for this application).

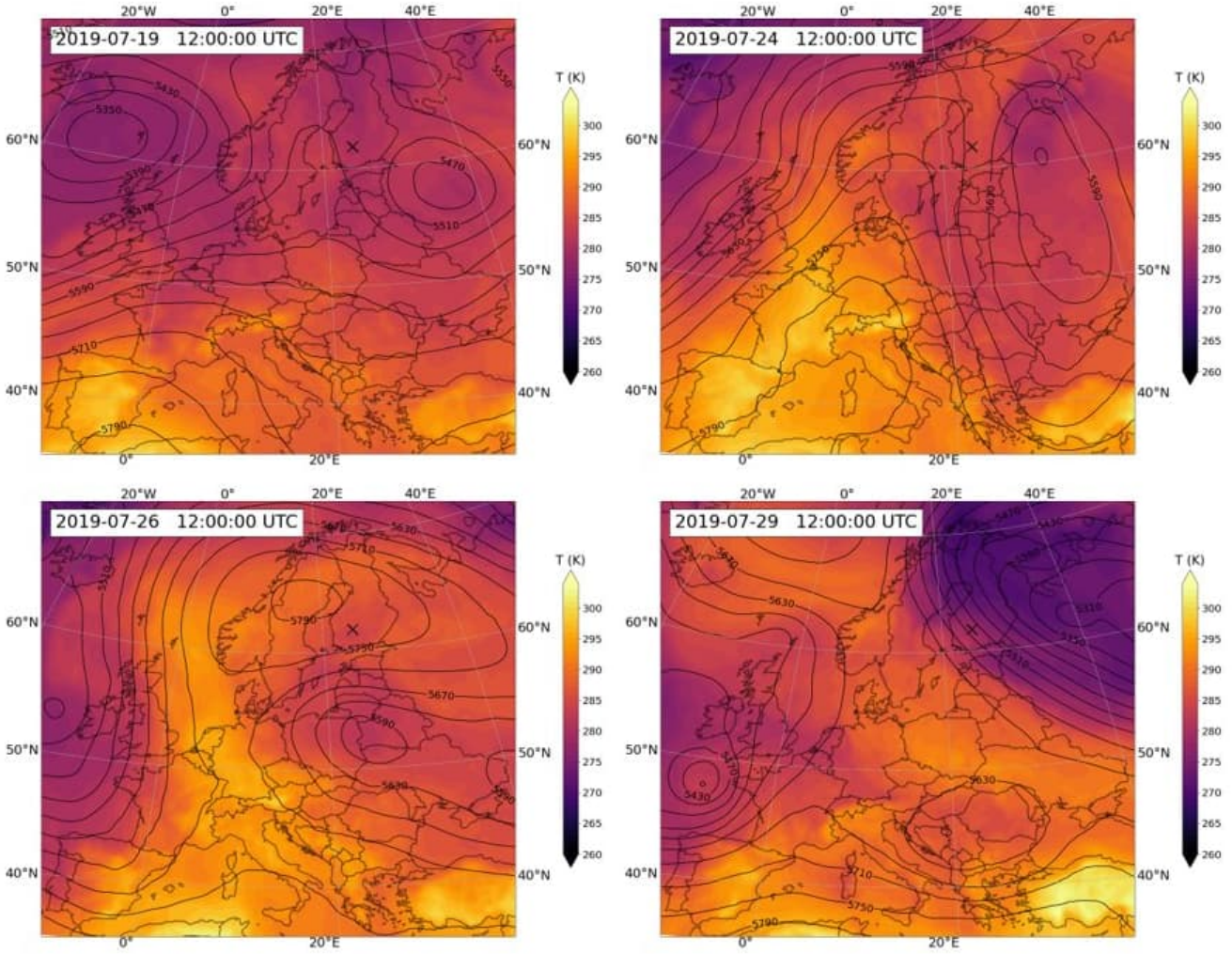

Figure 3: Geopotential height (m a.s.l.) at 500 hPa and air temperature (K) at 850 hPa for 4 days during the heat wave period (19-28 July). Data are taken from ERA5 reanalysis (available at cds.climate.copernicus.eu). The black cross denotes the location of the SMEAR-II station.

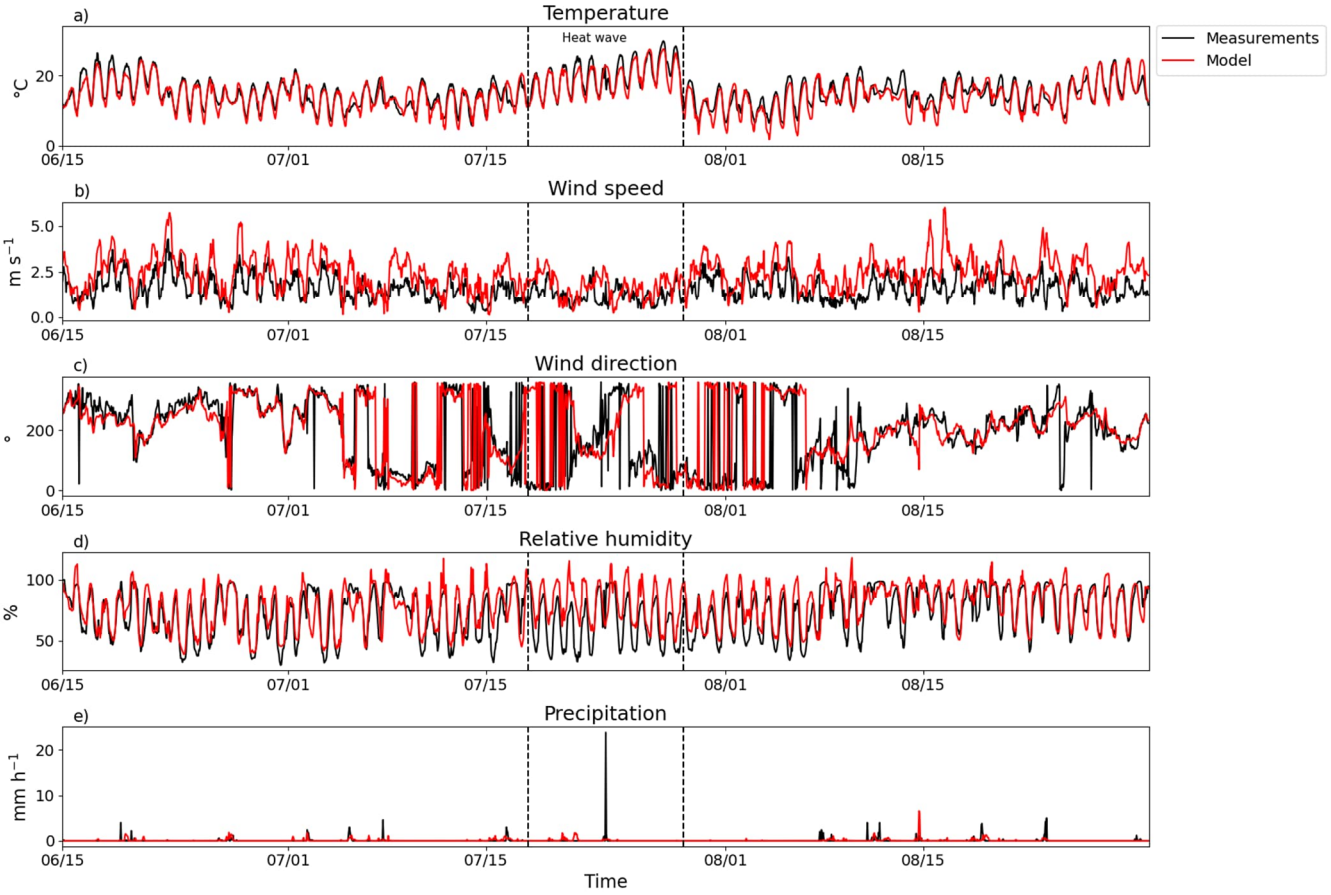

Figure 4: Hourly comparison of different meteorological parameters at the SMEAR-II station. From the top to the bottom: a) temperature (°C), b) wind speed (m s^{-1}), c) wind direction (°), d) relative humidity (%) and e) precipitation (mm h^{-1}). Black lines indicate the measurement data and red lines the model data. The dashed lines delimit the periods with sustained elevated temperature, denote here as "heat wave".

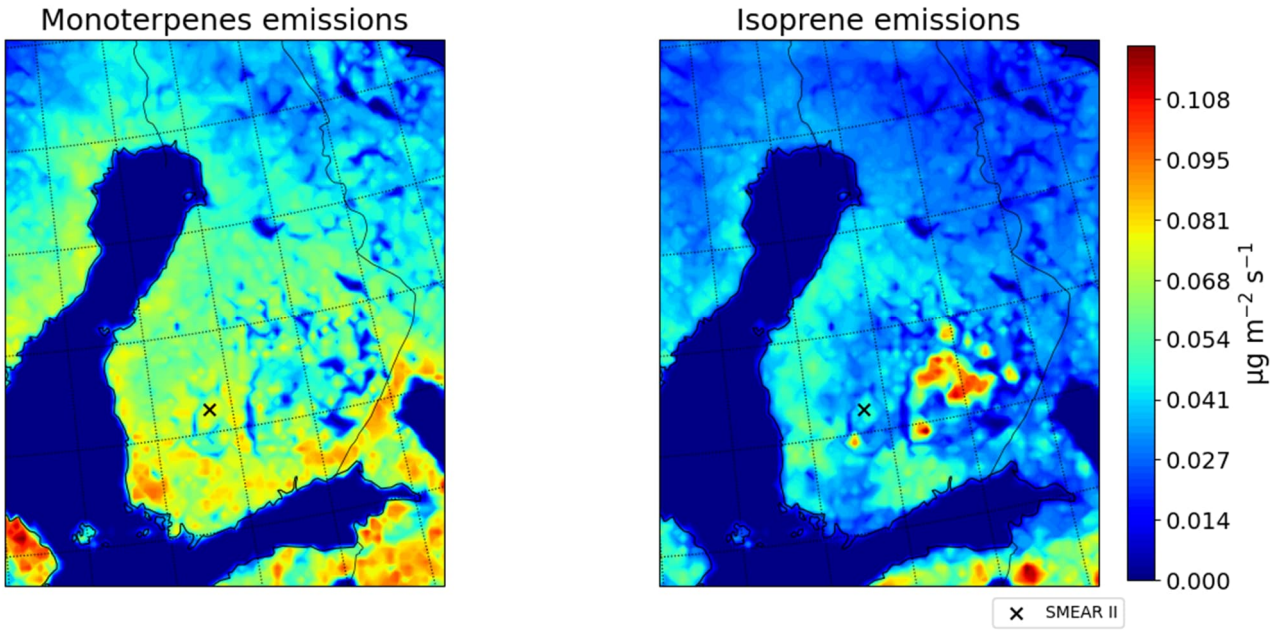

Figure 5: Average spatial distribution of monoterpenes (left) and isoprene (right) emissions (µg m $^{-2}$ s^{-1}) for the summer of 2019 (15 Jun–30 Aug 2019). The cross denotes the location of the SMEAR-II station. Monoterpenes represent here the sum of all the available terpenes species.

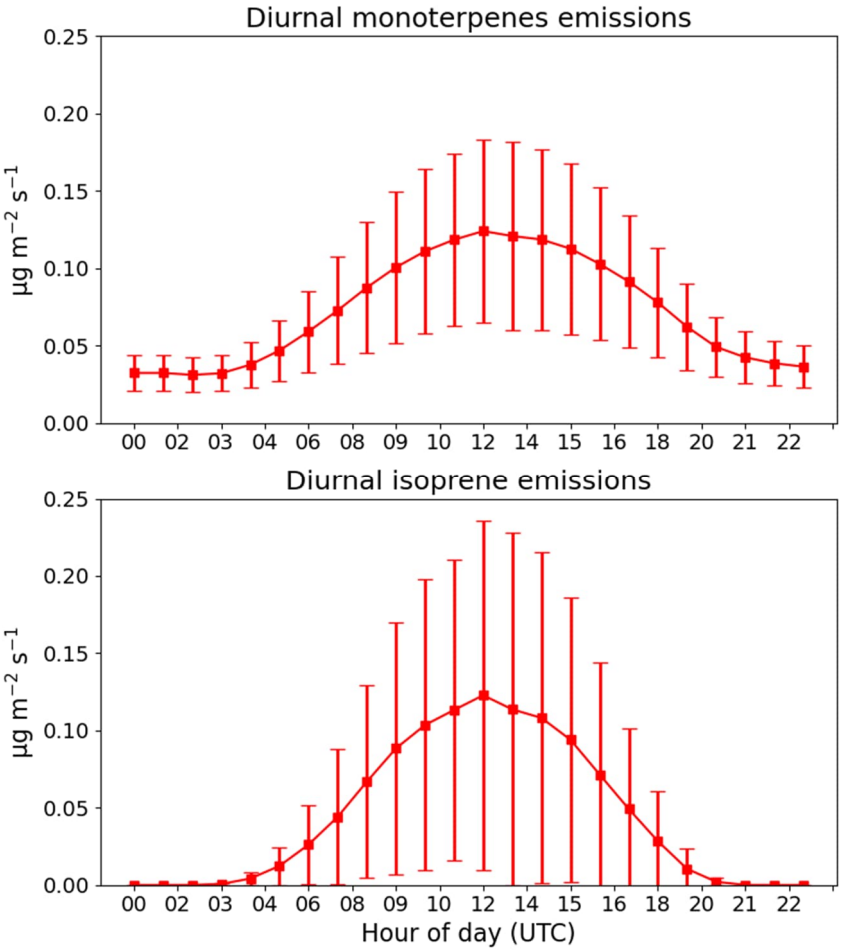

Figure 6: Average diurnal variation of monoterpenes (upper panel) and isoprene (lower panel) emissions (µg m^{-2} s) for the summer of 2019 (15 Jun–30 Aug 2019) at the SMEAR-II station. The extent of the red bars denotes the one standard deviation (1σ). Monoterpenes represent here the sum of all the available terpenes species.

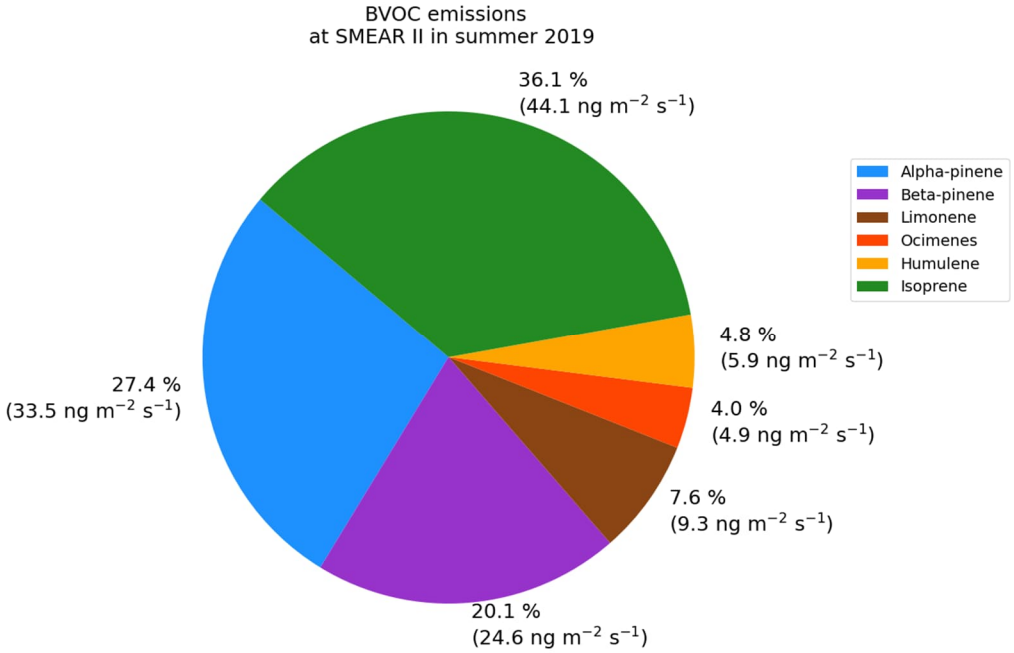

Figure 7: Average relative contribution of the BVOCs species as predicted by the MEGAN model for the summer of 2019 (15 Jun–30 Aug 2019) at the SMEAR-II station. Units are in ng m^{-2} s^{-1}.

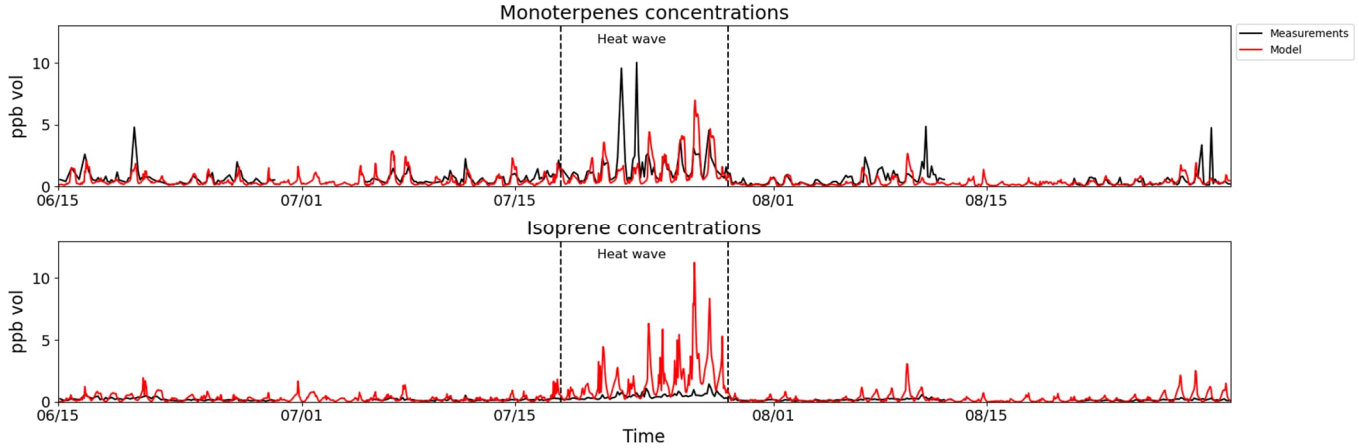

Figure 8: Hourly comparisons of model (red) and measured (black) air concentrations of a) isoprene and b) monoterpenes (sum of terpenes) at the SMEAR-II station. Units are in ppb vol. The dashed lines delimit the periods with sustained elevated temperature, denote here as "heat wave".

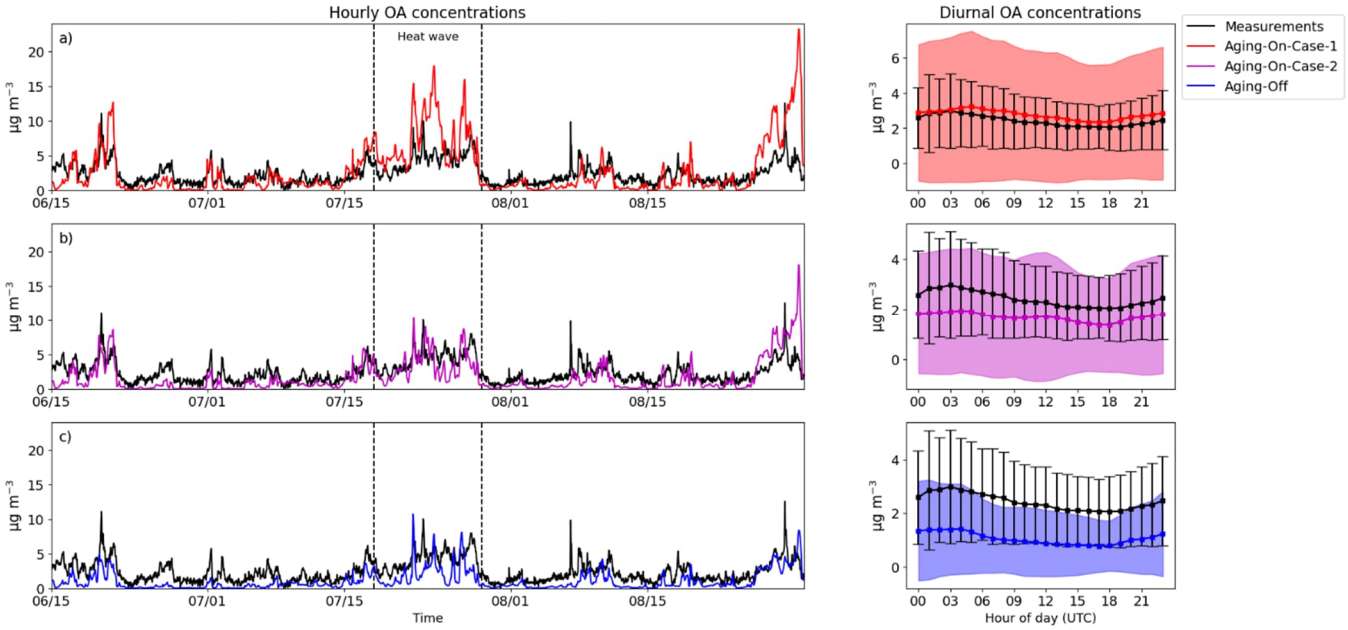

Figure 9: Model (different colors) and measured (black) air concentrations of OA for the a) Aging-On-Case-1, b) Aging-On-Case-2 and c) Aging-Off BSOA schemes. Hourly (left) and diurnal (right) comparisons at the SMEAR-II station. The dashed lines delimit the periods with sustained elevated temperature, denote here as "heat wave". The extent of the bars and the shaded areas denotes the one standard deviation (1σ). Units are in µg m^{-3}.

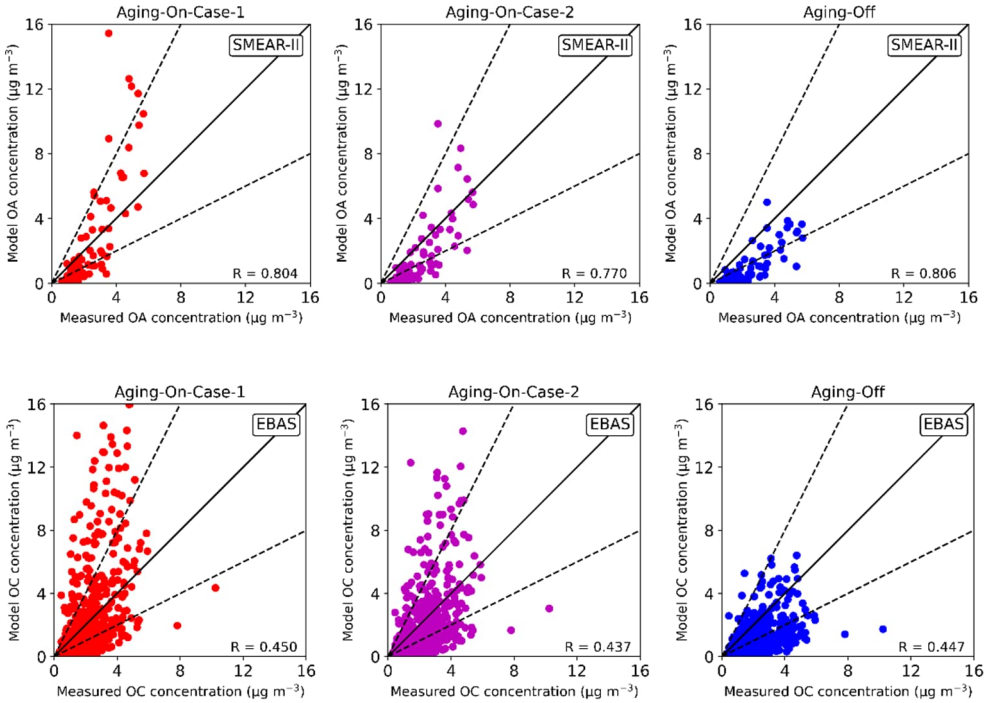

790

Figure 10: Model (y-axis) and measured (x-axis) air concentrations of OA for the Aging-On-Case-1 (left), b) Aging-On-Case-2 (center) and c) Aging-Off (right) BSOA schemes at the SMEAR-II station (upper pane, daily averages) and at available EBAS sites (bottom panel). Solid line indicates the 1:1 line. The dashed lines delimit 1:2 and 2:1 line. Units are in µg m-3. Data from the EBAS database has a time resolution varying from 4 hours to 1 week, depending on the specific site.

795

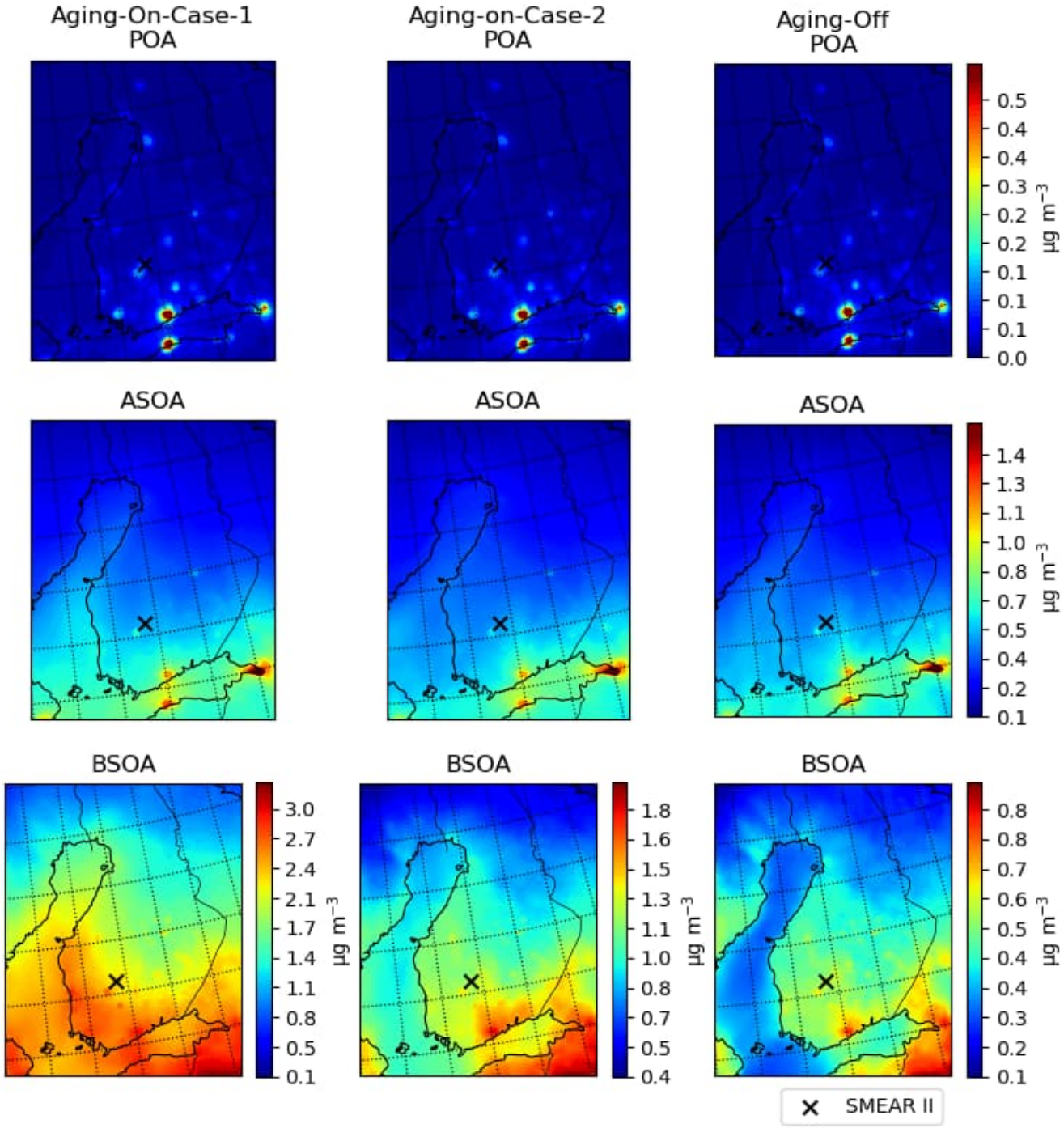

Figure 11: POA (top panel), ASOA (middle panel) and BSOA (bottom panel) average concentrations during the summer of 2019 (15 Jun–30 Aug 2019) and for the Aging-On-Case-1 (left), Aging-On-Case-2 (center) and the Aging-Off (right) BSOA schemes. The cross denotes the location of the SMEAR-II station. Units are in µg m^{-3}. A different scale in used for the BSOA panel (bottom panel) to facilitate the comprehensions of the panel.

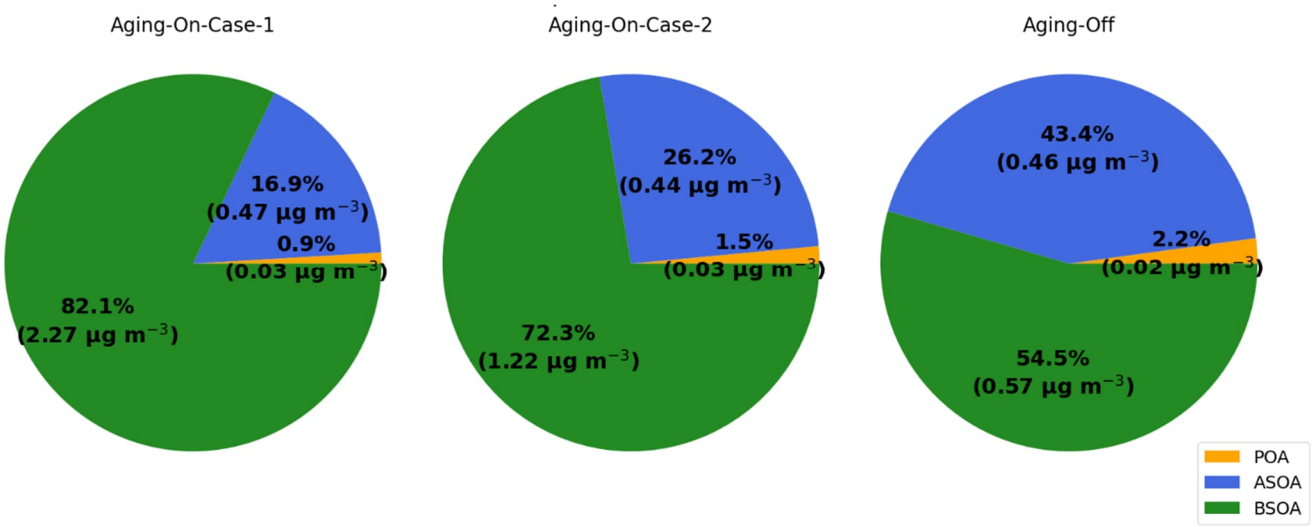

Figure 12: POA (orange), ASOA (blue) and BSOA (green) modeled average relative contribution to the total OA fraction for the summer of 2019 (15 Jun–30 Aug 2019) and for the Aging-On-Case-1 (left), b) Aging-On-Case-2 (center) and c) Aging-Off (right) BSOA schemes. Absolute concentrations are reported along with their relative contribution to the total OA.

805

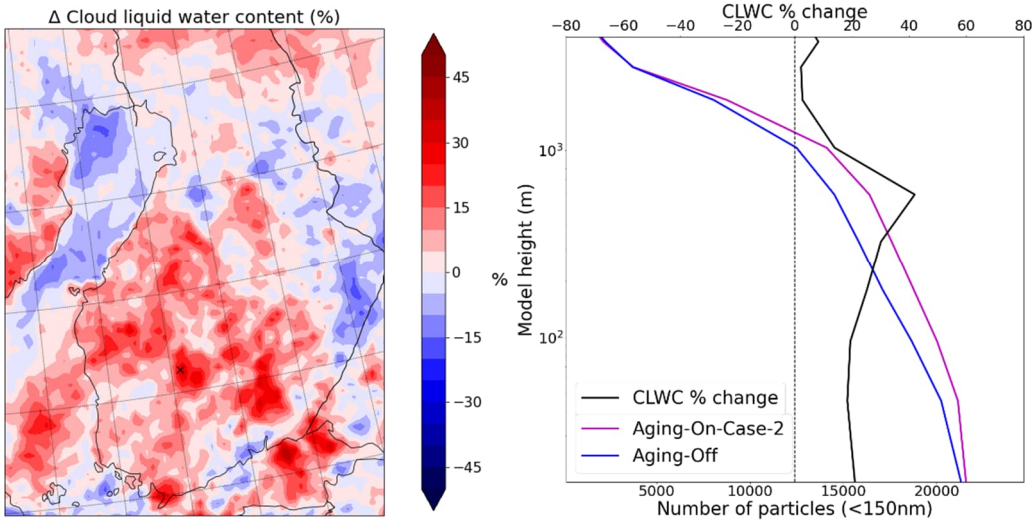

Figure 13: Integrated (vertical) differences in Cloud Liquid Water Content (left) over the high-resolution domain (10km). Vertical profile of particles below 150 nanometers in the Aging-On-Case-2 and Aging-Off simulations and of the relative changes in Cloud Liquid Water Content (right) over the SMEAR-II site (average of a 3x3 kilometers cell). The relative changes are reported here as ((Aging-On-Case-2 - Aging-Off) / Aging-Off) * 100.

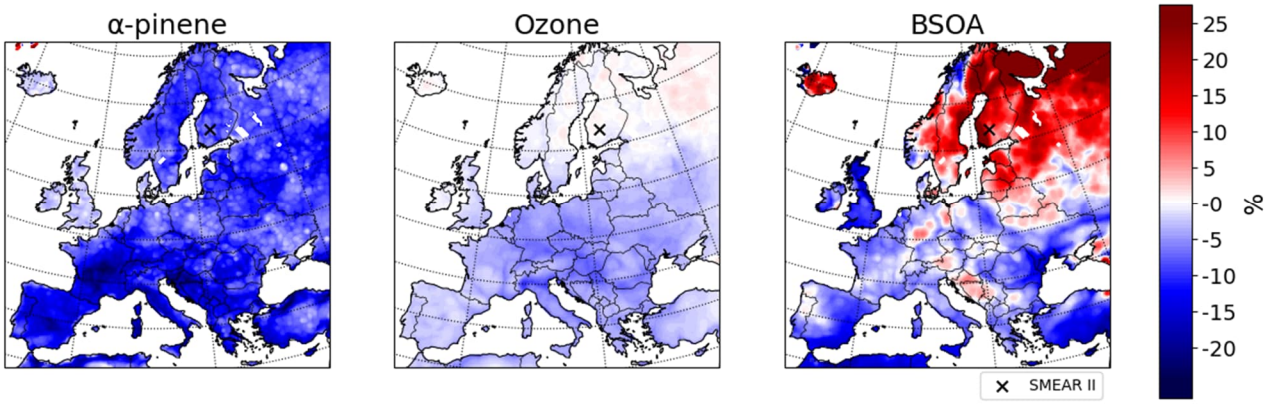

Figure 14: Daytime average (08 - 20 LT) relative changes in $C_{10}H_{16}$ (alpha-pinene) air concentrations, Ozone and BSOA concentrations with and without isoprene emissions. The relative changes are calculated as ((C_5H_8-emissions-Off - Aging-On-Case-2) / Aging-On-Case-2) * 100.

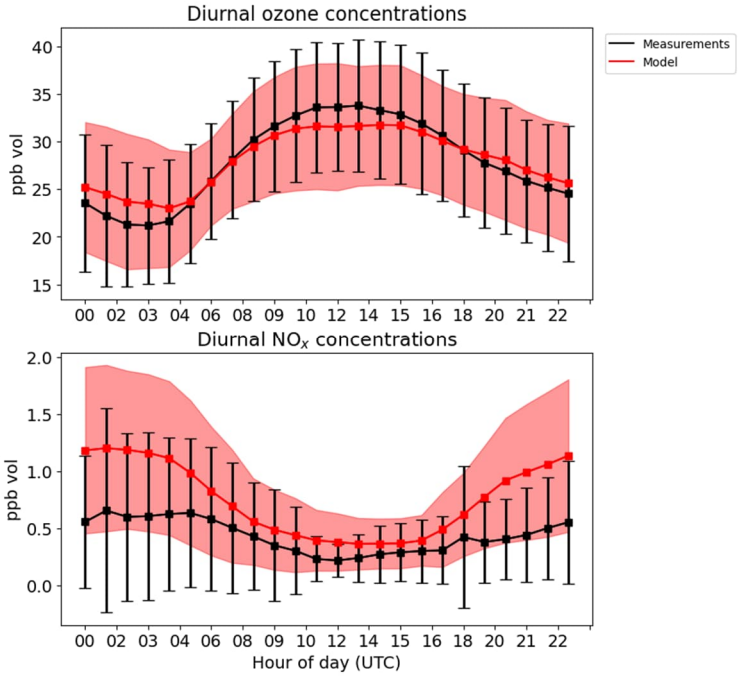

Figure 15: Diurnal variation of O_3 and NO_x at the SMEAR-II site (from 15 June until 30 August of 2019). The extent of the bars and the shaded areas denotes the one standard deviation (1σ). Measurements data are shown in in black and model data in red. Units are in ppb vol.

Table 1: Reaction rates constant of BSOA aging as used in the different sensitivity tests. The schematic of the aging scheme is reported in Figure 2.

Sensitivity Test	Aging (see Figure 2)
Aging-On-Case-1	1 x 10^{-11} molecule^{-1} cm^3 s $^{-1}$
Aging-On-Case-2	4 x 10^{-12} molecule^{-1} cm^3 s $^{-1}$
Aging-Off	0 molecule^{-1} cm^3 s $^{-1}$
C_5H_8-emissions-Off	4 x 10^{-12} molecule^{-1} cm^3 s $^{-1}$

Table 2: Statistical metrics used for model evaluation. M_i and O_i stand for modeled and observed values, respectively, and N is the total number of paired values.

Metric	Definition
Mean Bias (MB)	$MB = \frac{1}{N}\sum_{i=1}^{N}(M_i - O_i)$
Mean Gross Error (MGE)	$ME = \frac{1}{N}\sum_{i=1}^{N}\lvert M_i - O_i\rvert$
Root Mean Square Error (RMSE)	$RMSE = \sqrt{\frac{1}{N}\sum_{i=1}^{N}(M_i - O_i)^2}$
Index of Agreement (IOA)	$IOA = 1 - \frac{N \cdot RMSE^2}{\sum_{i=1}^{N}\left(\lvert M_i - \overline{O}\rvert + \lvert O_i - \overline{O}\rvert\right)^2}$
Pearson Correlation Coefficient (r)	$r = \frac{\sum_{i=1}^{N}(M_i - \overline{M})\cdot(O_i - \overline{O})}{\sqrt{\frac{1}{N}\sum_{i=1}^{N}(M_i - \overline{M})^2}\cdot\sqrt{\frac{1}{N}\sum_{i=1}^{N}(O_i - \overline{O})^2}}$
Mean Fractional Bias (MFB)	$MFB = \frac{1}{N}\sum_{i=1}^{N}\frac{2\cdot(M_i - O_i)}{M_i + O_i}$
Mean Fractional Error (MFE)	$MFE = \frac{1}{N}\sum_{i=1}^{N}\frac{2\cdot\lvert M_i - O_i\rvert}{M_i + O_i}$

Table 3: Model evaluation for the meteorological parameters (from 15 June until 30 August of 2019). Statistics is performed at 1-hour time resolution.

Variable	MB	MGE	RMSE	IOA (-)	r (-)
T (º C)	-0.7	1.6	2.0	1.0	0.9
Wind speed (m s^{-1})	0.8	0.9	1.1	0.6	0.6
Water vapor mixing ratio (g kg^{-1})	0.2	0.9	1.1	0.9	0.8

Table 4: Model evaluation for the BVOCs species isoprene and monoterpenes at the SMEAR II station (from 15 June until 30 August of 2019). Statistics is performed at 1-hour time resolution.

Variable	Mean measurements	Mean model	MB	MGE	r (-)
Monoterpenes (ppb)	0.8	0.6	-0.2	0.4	0.5
Isoprene (ppb)	0.2	0.5	0.3	0.3	0.6
O_3 (ppb)	27.9	27.9	-0.1	5.6	0.5
NO_x (ppb)	0.4	0.8	0.3	0.5	0.4

Table 5: Model evaluation for OA as predicted by the three BSOA schemes at the SMEAR II station (from 15 June until 30 August of 2019). Statistics is performed at 1-hour time resolution.

Variable	Mean	MB	MGE	RMSE	MFB	MFE
Aging-On-Case-1 (µg m^{-3})	2.8	0.3	1.8	2.9	-0.5	0.9
Aging-On-Case-2 (µg m^{-3})	1.7	-0.7	1.4	1.9	-0.8	1.0
Aging-Off (µg m^{-3})	1.1	-1.4	1.5	1.9	-1.1	1.1
Obs (µg m^{-3})	2.5	-	-	-	-	-

Supplement

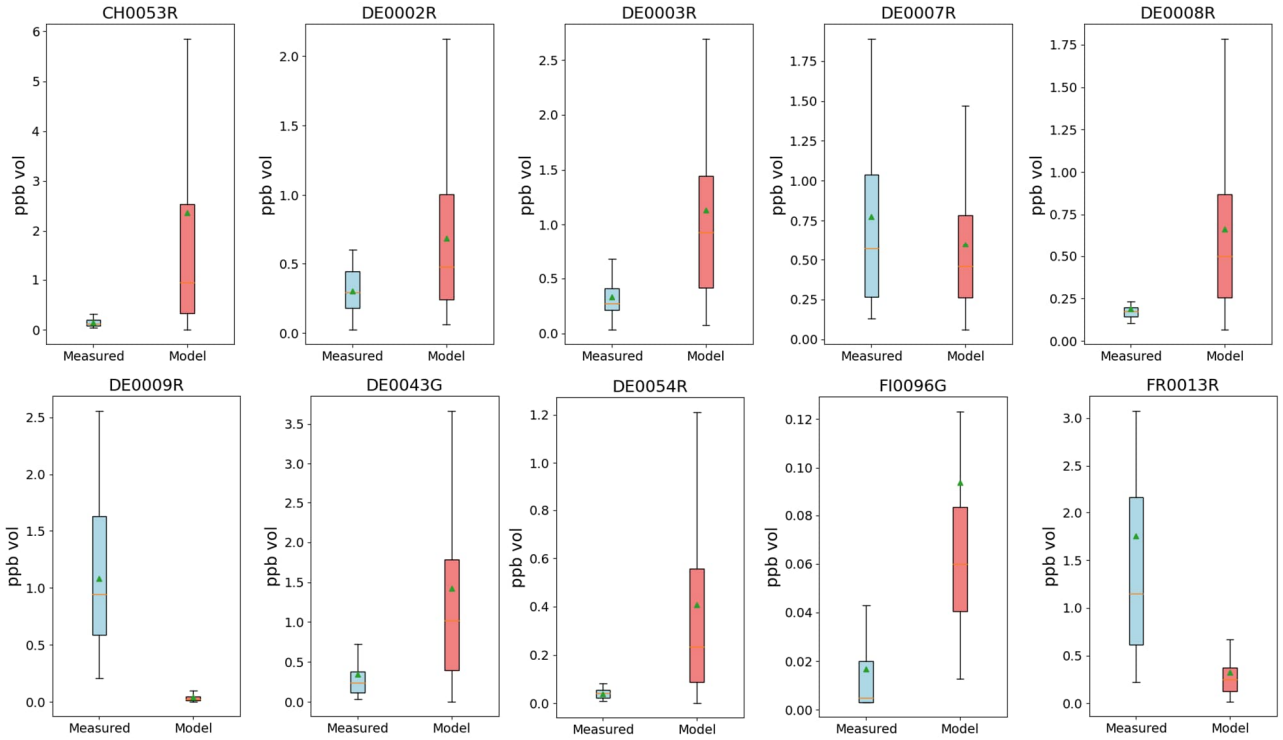

Figure S1: Comparisons of modeled (red) and measured (blue) air concentrations of isoprene as available from the EBAS database. Measurement time resolution varies from is 1 hours to 4 days depending on the specific station. Units are in ppb vol.

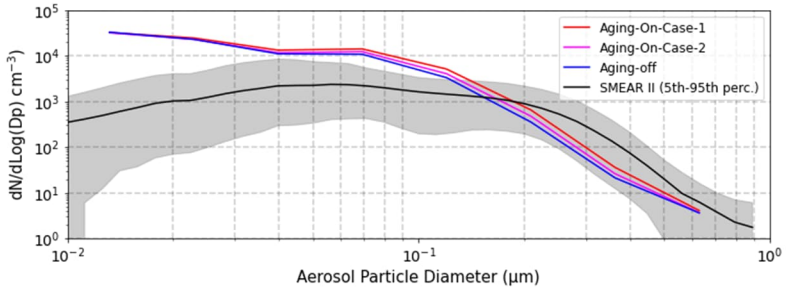

Figure S2: Measured (black) and modelled (various colors) median size distribution comparison at the SMEAR-II stations. The shaded areas indicated the 5th and 95th interquartile range.

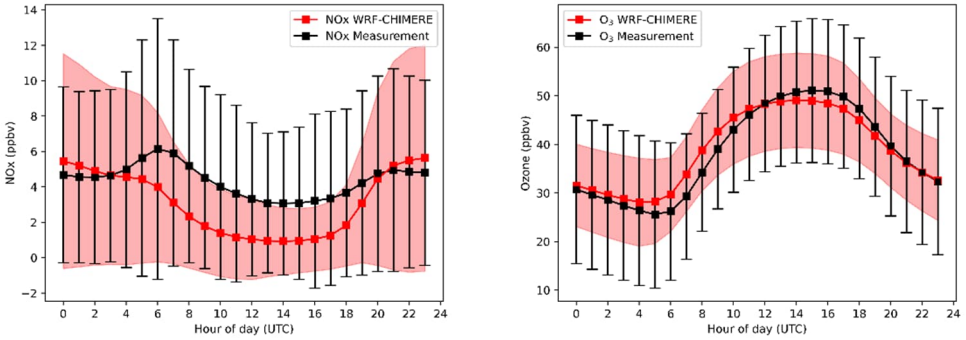

Figure S3: Diurnal variation of O_3 and NO_x at available Air Quality e-Reporting rural sites (from 15 June until 30 August of 2019). Number of stations are 271 for NOx and 350 for O_3. The extent of the bars and the shaded areas denotes the one standard deviation (1σ). Measurements data are shown in in black and model data in red. Units are in ppb vol.

Table S1: EBAS stations (from https://ebas.nilu.no/) used for the organic carbon (OC) comparison on the coarse resolution grid (30km).

Site	Latitude (deg)	Longitude (deg)
CZ0003R	49.5734	15.0803
DE002R	52.8022	10.7594
DE003R	47.9147	7.9086
DE0007R	53.1667	13.0333
DE0008R	50.6500	10.7667
DE0009R	54.4368	12.7249
DE0044R	51.5255	12.9277
FR0008R	48.5000	7.1333
FR0009R	49.9000	4.6333
FR0013R	43.6167	0.1833
FR0022R	48.5622	5.5056
FR0023R	44.5694	5.2790
FR0024R	47.8319	-1.8363
FR0025R	46.8147	2.6100
NO0002R	58.3885	8.2520
NO0039R	62.7833	8.8833
NO0056R	60.3724	11.0781
PL0005R	54.1500	22.0667
PL0009R	53.6621	17.9340

865

Table S2: EBAS stations (from https://ebas.nilu.no/) used for the isoprene air concentration comparison on the coarse resolution grid (30km).

Site	Latitude (deg)	Longitude (deg)
CH0053R	47.1896	8.1754
DE0002R	52.8022	10.7594
DE0003R	47,9147	7,9086
DE0007R	53.1666	13.0333
DE0008R	50.6500	10.7666
DE0009R	54.4368	12.7249
DE0043G	47.8014	11.0096
DE0054R	47.4165	10.9796
FI0096G	67.9733	24.1161
FR0013R	43.6166	0.1833

870

Table S3: Model evaluation for organic carbon (OC) as predicted by the three BSOA schemes at the EBAS stations (from https://ebas.nilu.no/) Table S1.

Variable	Mean	MB	MGE	RMSE	MFB	MFE
Aging-On-Case-1 (µg m^{-3})	3	0.63	1.84	2.88	0.56	1.65
Aging-On-Case-2 (µg m^{-3})	2.4	-0.13	1.52	1.52	-0.08	1.37
Aging-Off (µg m^{-3})	1.3	-1.1	1.34	1.68	-0.86	1.16
Obs (µg m^{-3})	2.4	-	-	-	-	-

875 **Table S4: Model evaluation for O_3 and NO_x concentrations against measurements from the Air Quality e-Reporting rural sites. Number of stations are 271 for NOx and 350 for O_3.**

Variable	Mean measurements	Mean model	MB	MGE	r (-)
O_3 (ppb)	38.4	39.5	1.05	7.38	0.55
NO_x (ppb)	4.4	2.5	-1.8	2.5	0.45